Supporting Information

Leveraging Steric Moieties for Kinetic Control of DNA Strand Displacement Reactions

Drew Lysne,[a] Tim Hachigian,[a] Chris Thachuk,[b] Jeunghoon Lee,[a,c,] and Elton Graugnard. [a,d,]**

[a] Micron School of Materials Science & Engineering
Boise State University, 1910 University Dr., Boise, ID, 83725, USA.
[b] Paul G Allen School of Computer Science and Engineering
University of Washington, Paul G. Allen Center, 185 E Stevens Way NE, Seattle, WA 98195-2350, USA.
[c] Department of Chemistry and Biochemistry
Boise State University, 1910 University Dr., Boise, ID, 83725, USA.
[d] Center for Advanced Energy Studies, Idaho Falls, ID, 83401, USA.

* To whom correspondence should be addressed

Table of Contents

Materials and Methods

DNA Sequences and Design

The sequences featured here were designed, in part, based on the work of Wang et al.[1], and also in part, on the work of Zhang et al.[2] They were specifically formulated using an in-house sequence evolution software that minimizes secondary structure and crosstalk between all strands. NUPACK was then used to validate the complex formations as being thermodynamically favorable at the targeted 25 °C experimental temperature and comparable salt concentration of 0.05M Na+ and 0.0125 Mg++.

Buffer Conditions

All DNA oligonucleotides were ordered dry from IDT and resuspended according to IDT's recommended resuspension process. The process included an initial spinning of each tube, which we performed at 12,000 rpm for three minutes. After spinning, the oligos were dissolved into 1x TE buffer (10 mM Tris HCl, 1 mM EDTA, pH of approximately 8.0, purchased as 100x stock from Sigma Aldrich) and stored at 4 °C in approximately 100 μM concentrations. Preceding experiments, oligos were transferred to 1x TE buffer with a 12.5 mM concentration of $MgCl_2$. Purifications were performed at approximately 20 °C. Low salt experiments were run in a 1x TE, 1.25 mM $MgCl_2$ buffer solution, high salt experiments were run in a 1x TE, 125 mM $MgCl_2$ buffer solution and the rest of experiments were run in a default 1x TE, 12.5 mM $MgCl_2$ buffer solution at 25 °C.

Substrate Purification

Unfunctionalized DNA oligonucleotides were all purified by IDT using their default standard desalting option. Fluorophore functionalized dye and quencher oligos were all HPLC purified by IDT. Concentrations of oligos were determined using a Fisher Scientific Nanodrop instrument and an oligo extinction coefficient.

Oligos were mixed at nominal 20 μM concentrations at the experimental salt concentration of 12.5 mM $MgCl_2$ and annealed in an Eppendorf Mastercycler Gradient thermocycler at 95 °C for 5 minutes before ramping down to 20 °C at a constant rate over the course of 90-minute period.

Experimental complexes were further purified using non-denaturing polyacrylamide gel electrophoresis (PAGE). 1xTBE gels with 12.5 mM Mg++ were casted into a 5%/8% stacked configuration. The complexes were run at 120 V for 3 h in a Hoefer SE260 Mighty Small II Deluxe Mini Vertical Protein Electrophoresis Unit. Gels were imaged, and bands cut out to elute in 1x TE, 12.5 mM $MgCl_2$ buffer for two days. After the bands were eluted, the supernatant was extracted via pipette and transferred to a new Eppendorf lo-bind tube. This procedure separates most of the gel fragments from the purified complexes. The transferred supernatant was then spun down at 12,000 rpm for three minutes to settle the remainder of the gel fragments and this supernatant was extracted slowly and carefully leaving a small layer of solution on top of the precipitated gel sediments.

Measurements

Spectrofluorimetry studies were performed using an Agilent Cary Eclipse fluorescence spectrophotometer and Varian Cary Eclipse fluorescence spectrophotometer pair equipped with temperature controllers and four-seated sample exchangers. Slit widths of 5 and 10 nm were used for the excitation and emission slits respectively. Tetrachlorofluorocein (TET) dyes excited at 522 nm and fluorescing at 539 nm, and Iowa Black FQ quenchers with peak absorbance at 531 nm, were used in all complexes. Instruments were thus set to excite at 522 nm while collecting at

539 nm. The reaction volume for all experiments was 1.5 mL and took place within 3 mL, polymethyl methacrylate (PMMA) disposable cuvettes. Cuvettes were capped to reduce intensity creep due to evaporation.

Sample Details

Before running any experiments, a working solution containing the invading strand was prepared and then poly-T was mixed with this solution. Before each experiment the absorbance of the complex solutions would be measured using a Fisher Scientific Nanodrop instrument. These absorbances were paired with the proper extinction coefficients for each complex to calculate the concentration which was then used to calculate the volume of complex to add to cuvettes for experiments. All experiments were run at 2 nM concentrations of reporter complexes and invader strands. To ensure that all complex concentrations were the same, and that larger reporter complex concentrations weren't being over-estimated, and thus causing our studied phenomena of decreased rate constant with increased number of arms, cuvettes were removed towards the end of all experimental runs and a small 2 μL shot of 100 μM invading strand was added to each cuvette and then placed back in the instrument to continue tracking. This is seen as the sudden decrease in signal followed by the sudden increase in signal of kinetics curves from 300-600 minutes featured in **Figures S11** through **S19**.

In initial experiments after adding a shot of 2 μL invader strand at the end of the experiment, the intensities would jump up 25% to the expected max intensity values of each instrument for that concentration of dye. It was suspected that the invader strand concentration was not actually as high as initially diluted to, and since the poly-T is added after, the concentration could no longer be found. To account for this difference in final intensity (and achieve 1:1 stoichiometry) an excess of 25% invader was calculated into the mixing recipes. This change led to just minor intensity jump with the addition of the invader strand shot at the end of experiments, indicating a nominal 1:1 stoichiometry.

There are variations in the final intensity of the kinetics curves shown in **Figures S11** and **S19**. The main source that can be observed is from the difference in arbitrary intensities from the two different instruments that were used. One instrument shows intensity peaking at about 35 a.u. while the other around 45 a.u. Besides this there is just minor variations and nothing that suggests the concentrations were somehow being increasingly (or decreasingly) mis-calculated with increasing complex size.

Carrier Strands

Sample dilution through pipette tip loss was found to be more prominent with the single strand invader and not as pronounced in the hybridized complexes. For this reason, a 20 nt poly-t strands were added to the invader at a 1 μM concentration to help mitigate inconsistent losses.

Strand Sequences

Unconstrained and Constrained Complex Sequences

Table S1 These strands were used for all experiments with 30 base pair auxiliary arms. All unconstrained complexes with 30 base pair auxiliary arms used these strands exclusively. Constrained complexes utilized the internal toehold quencher strand (IT-Quencher), and all full-auxiliary strands (AuxN). Unconstrained truncated complexes did not utilize these strands to create complexes.

Complexes	Strand Name	Strand Sequence (5' – 3')
Unconstrained and Constrained Complexes with 30 Base Pair Arms	Dye+Aux	/5TET/TCAACCACATAACTTTCCCTCCACACATTCCATACACCATTCTCTCCTCC
	IT-Quencher	GGGAGTGTGTAGAGTGAGGGTTGTGAGAGAGTAGTGAAGGGAAAGTTATGTGGTTGA/3IABkFQ/
	Dye	/5TET/TCAACCACATAACTTTCCCT
	Quencher	GTAGTGAAGGGAAAGTTATGTGGTTGA/3IABkFQ/
	Invader	TCAACCACATAACTTTCCCTTCACTAC
	Aux0	TCTCTCACAACCCTCACTCTACACACTCCC
	Aux1	GGAGGAGAGAATGGTGTATGGAATGTGTGGTGGGTTGGGATGGTATGAGAAAAGAGTGGG
	½ Aux1	GGAGGAGAGAATGGTGTATGGAATGTGTGG
	Aux2	CCCACTCTTTTCTCATACCATCCCAACCCAGCCCAATTCCTTCCACTTTACCAACTACCC
	½ Aux2	CCCACTCTTTTCTCATACCATCCCAACCCA
	Aux3	GGGTAGTTGGTAAAGTGGAAGGAATTGGGCAGGGTAGGTTAAAGGGAGAAGGATGTTGGG
	½ Aux3	GGGTAGTTGGTAAAGTGGAAGGAATTGGGC
	Aux4	CCCAACATCCTTCTCCCTTTAACCTACCCTCCACTCACTTCTCTAACCCTAACACTTCCC
	½ Aux4	CCCAACATCCTTCTCCCTTTAACCTACCCT
	Aux5	GGGAAGTGTTAGGGTTAGAGAAGTGAGTGGTGGGAGGAAAAGGTATTGGGTATAGGTGGG
	½ Aux5	GGGAAGTGTTAGGGTTAGAGAAGTGAGTGG
	Aux6	CCCACCTATACCCAATACCTTTTCCTCCCAGCCCTACATCTTTCACATCTACAACCTCCC
	½ Aux6	CCCACCTATACCCAATACCTTTTCCTCCCA
	Aux7	GGGAGGTTGTAGATGTGAAAGATGTAGGGCATGGAAATAGTGGGTGTGAGGTAAGGAGGG
	½ Aux7	GGGAGGTTGTAGATGTGAAAGATGTAGGGC
	Aux8	CCCTCCTTACCTCACACCCACTATTTCCATCAACTTCCAACTCCCTACTCCATTTCACCC
	½ Aux8	CCCTCCTTACCTCACACCCACTATTTCCAT
	Aux9	GGGTGAAATGGAGTAGGGAGTTGGAAGTTGTTGAGGGATGAGTAATGGGTGAGATGAGGG
	½ Aux9	GGGTGAAATGGAGTAGGGAGTTGGAAGTTG
	Aux10	CCCTCATCTCACCCATTACTCATCCCTCAAGCCCTCTTCTTCATCACCAAACATACTCCC
	½ Aux10	CCCTCATCTCACCCATTACTCATCCCTCAA
	Aux11	GGGAGTATGTTTGGTGATGAAGAAGAGGGCAGGAGGTGATTGAGAGGATTGGAGATAGGG
	½ Aux11	GGGAGTATGTTTGGTGATGAAGAAGAGGGC
	½ Aux12	CCCTATCTCCAATCCTCTCAATCACCTCCT

Truncated Unconstrained External and Internal Toehold Complex Strands

Table S2 Truncated dye, quencher, and auxiliary strands. These strands were utilized to construct reduced mass complexes presented in **Figure 6** of the manuscript.

Complexes	Strand Name	Strand Sequence (5' – 3')
Unconstrained External and Internal Toehold Truncated 20 base pair Auxiliary Arm Complexes	IT-Quencher_20nt	AGAGTGAGGGTTGTGAGAGAGTAGTGAAGGGAAAGTTATGTGGTTGA/3IABkFQ/
	Dye+Aux_20nt	/5TET/TCAACCACATAACTTTCCCTCCACACATTCCATACACCAT
	Aux0_20nt	TCTCTCACAACCCTCACTCT
	Aux1_20nt	ATGGTGTATGGAATGTGTGGTGGGTTGGGATGGTATGAGA
	½ Aux1_20nt	ATGGTGTATGGAATGTGTGG
	Aux2_20nt	TCTCATACCATCCCAACCCAGCCCAATTCCTTCCACTTTA
	½ Aux2_20nt	TCTCATACCATCCCAACCCA
	Aux3_20nt	TAAAGTGGAAGGAATTGGGCAGGGTAGGTTAAAGGGAGAA
	½ Aux3_20nt	TAAAGTGGAAGGAATTGGGC
	Aux4_20nt	TTCTCCCTTTAACCTACCCTCCACTCACTTCTCTAACCCT
	½ Aux4_20nt	TTCTCCCTTTAACCTACCCT
	Aux5_20nt	AGGGTTAGAGAAGTGAGTGGTGGGAGGAAAAGGTATTGGG
	½ Aux5_20nt	AGGGTTAGAGAAGTGAGTGG
	½ Aux6_20nt	CCCAATACCTTTTCCTCCCA

Constrained Complex Connector Strand Sequences

Table S3 Connector and modified invader strands for constrained complex experiments. Connector strands (Aux_CN) were substituted in for internal toehold complex Aux 0 and ½ Aux strands from **Table S1** to construct constrained complexes illustrated in **Figure S4**.

Complexes	Strand Name	Strand Sequence (5' – 3')
Constrained Complex Connector Strands and Extended Invader	Aux_C1	GGAGGAGAGAATGGTGTATGGAATGTGTGGTCTCTCACAACCCTCACTCTACACACTCCC
	Aux_C2	CCCACTCTTTTCTCATACCATCCCAACCCATCTCTCACAACCCTCACTCTACACACTCCC
	Aux_C3	GGGTAGTTGGTAAAGTGGAAGGAATTGGGCTCTCTCACAACCCTCACTCTACACACTCCC
	Aux_C4	CCCAACATCCTTCTCCCTTTAACCTACCCTTCTCTCACAACCCTCACTCTACACACTCCC
	Aux_C5	GGGAAGTGTTAGGGTTAGAGAAGTGAGTGGTCTCTCACAACCCTCACTCTACACACTCCC
	Aux_C6	CCCACCTATACCCAATACCTTTTCCTCCCATCTCTCACAACCCTCACTCTACACACTCCC
	Extended Invader	TCAACCACATAACTTTCCCTTCACTACTCTCTCACAACCCTCACTCTACACACTCCC

Constructing Complexes

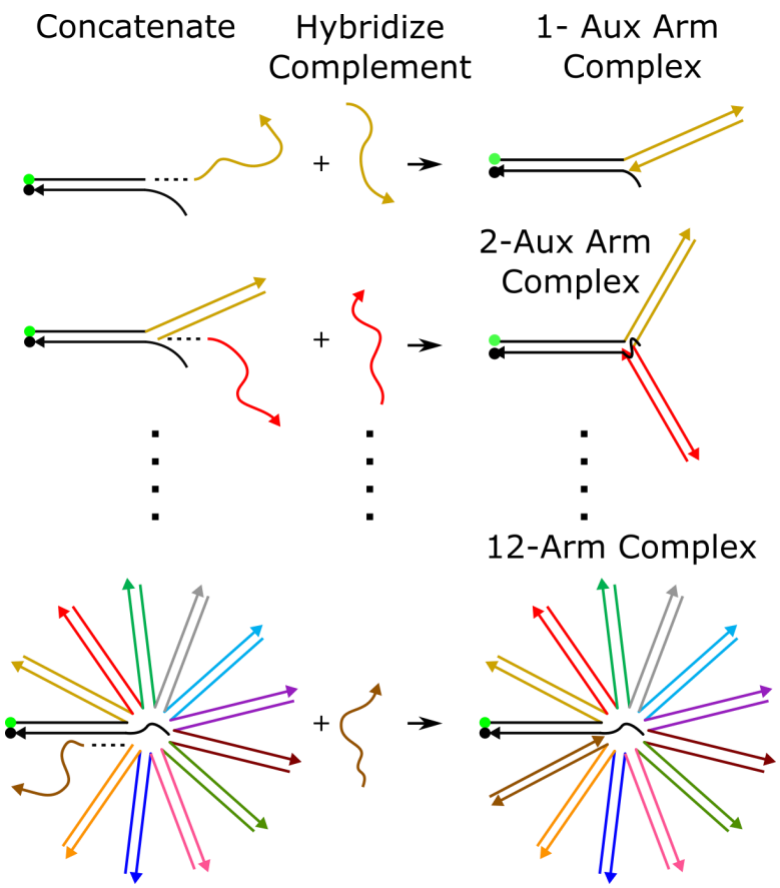

Figure S1 An unconstrained external toehold complexes help model the construction process. Constructing complexes from the base reporter involves concatenating a thirty-nucleotide sequence to the dye strand or previously added complementary strand and then hybridizing the concatenated strand to its complementary strand. Both external and internal toehold complexes were expanded to a limit of twelve auxiliary arms while constrained complexes were only expanded to a total of six arms.

Complex 2D Illustrations (Schematics)

Unconstrained External Toehold Complex

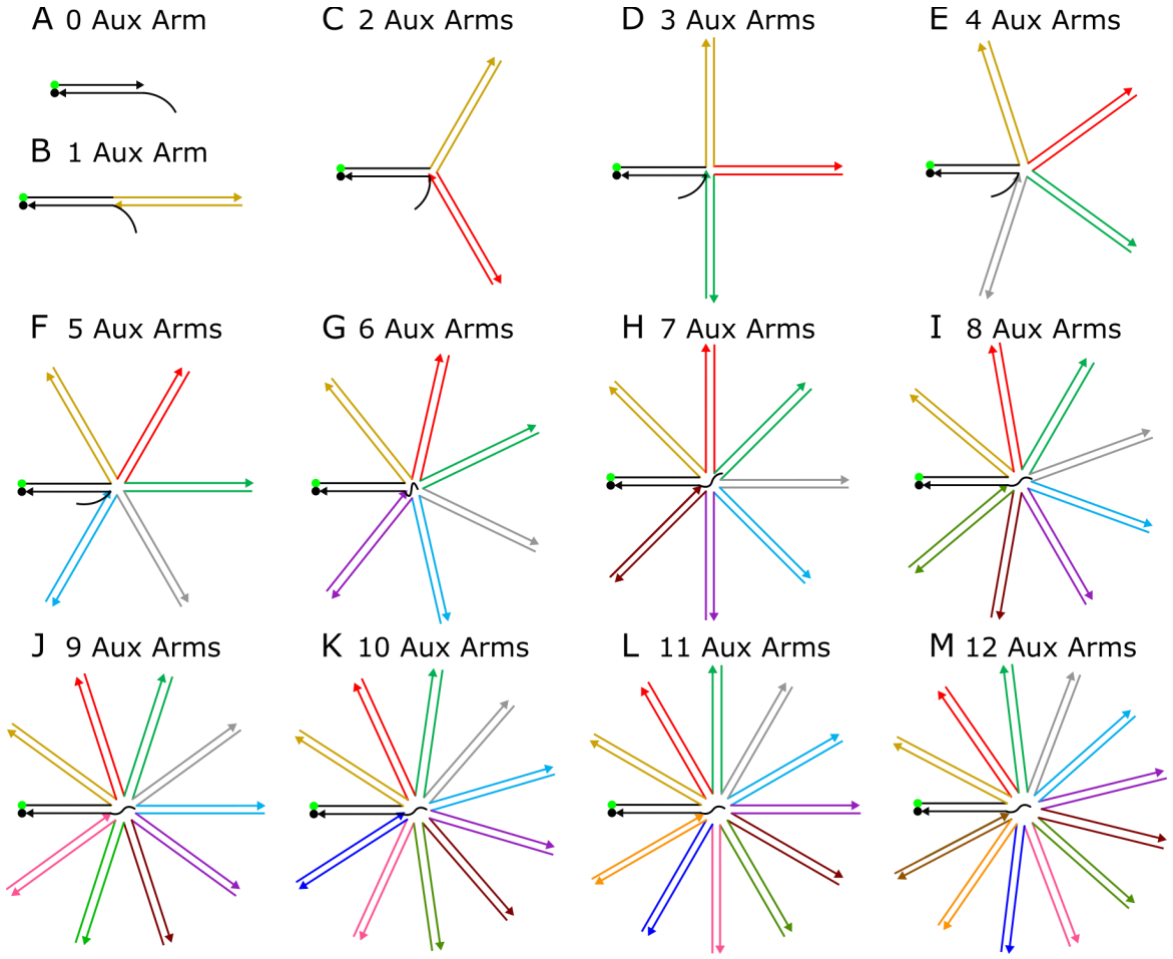

Figure S2 Two dimensional schematics of unconstrained external toehold complexes. The reporting duplex is shown in black on the left-hand side of the complex with the dye and quencher presented as green and black circles respectively. The toehold is represented by the black wavey portion of the quencher strand located in the junction. Auxiliary arms are incrementally added starting from 0 auxiliary arms at **A** to 12 auxiliary arms at **M**. Arms are color coded with the sequences in **Table S1**.

Unconstrained Internal Toehold Complexes

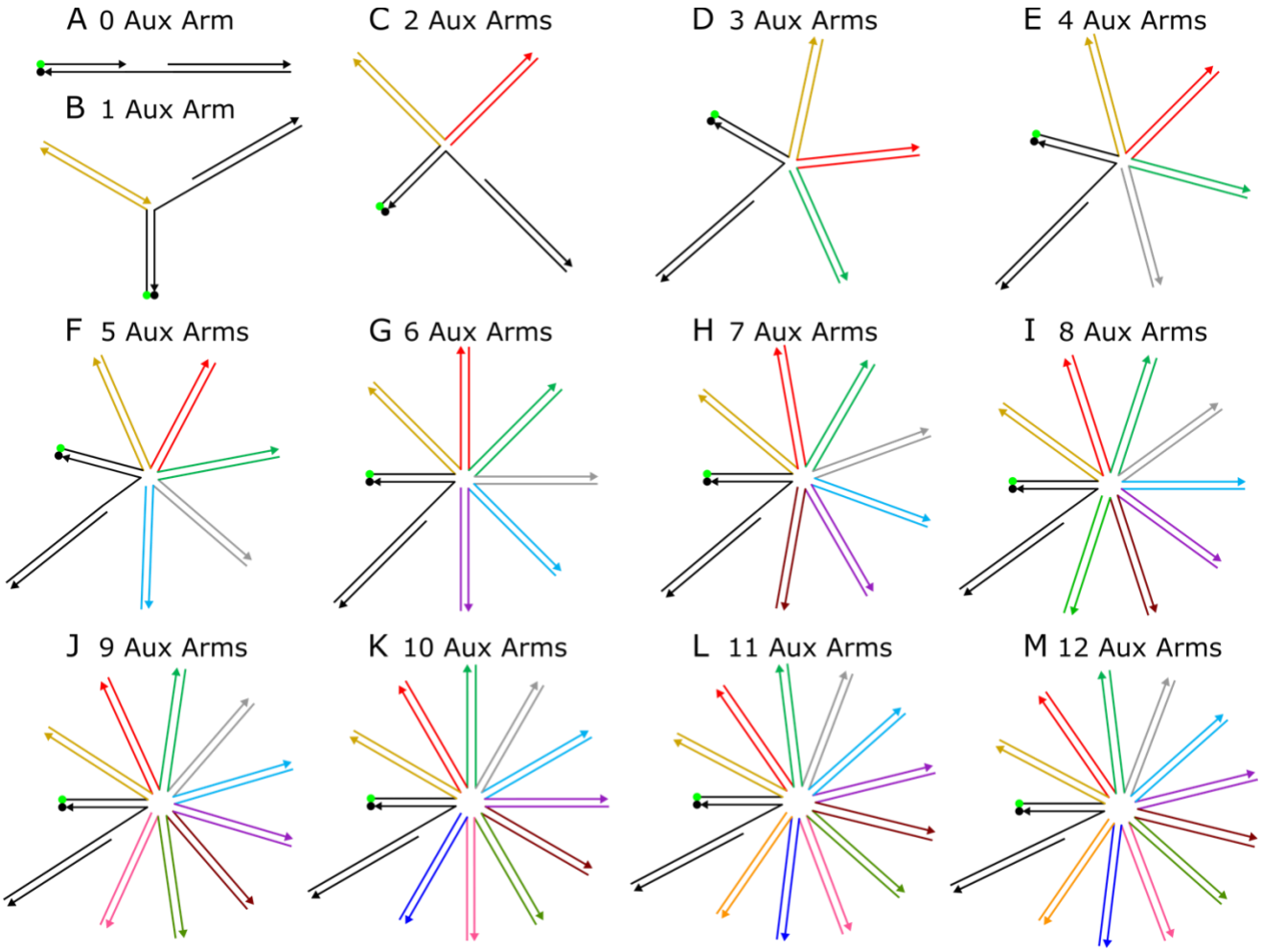

Figure S3 Two dimensional schematics of internal toehold complexes. The reporting duplex is shown in black on the left-hand side of the complex with the dye and quencher presented as green and black circles respectively. The toehold is represented by the black single line between double line section of the quencher strand. Auxiliary arms are incrementally added starting from 0 auxiliary arms at **A** to 12 auxiliary arms at **M**. Internal toehold complexes possess an additional duplex on the opposite end of the toehold from the reporting duplex. Besides the additional duplex on the opposite side of the toehold, internal toehold complexes are identical to their external toehold complex analogs. The arms in these schematics are color coded with the stands in **Table S1**.

Constrained Toehold Illustrations

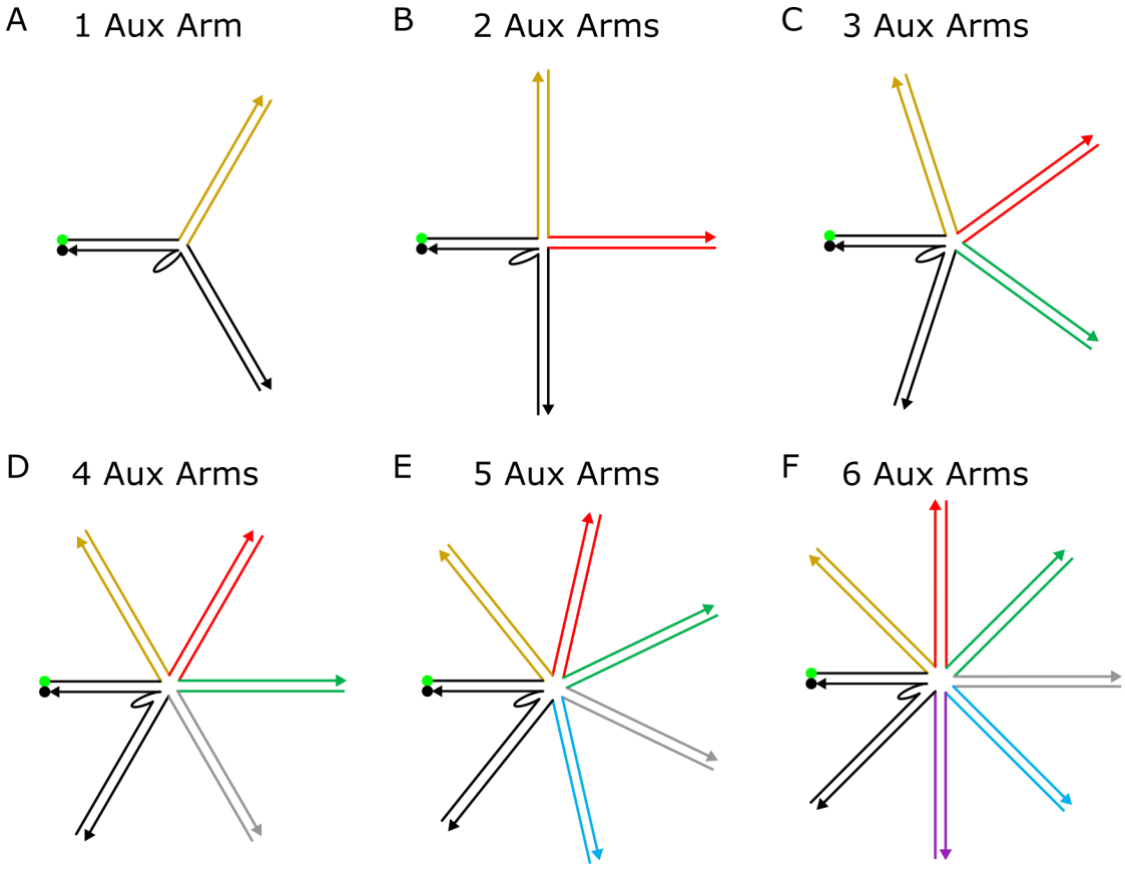

Figure S4 Two dimensional schematics of constrained complexes. Constrained complexes consist of the unconstrained internal toehold complex dye, quencher, and auxiliary strands, however, instead of possessing half-auxiliary strands, or Aux 0 strands, they utilize a concatenation of these two strands to connect the auxiliary domain of the internal toehold quencher with the final auxiliary strand of the complex. Connecting strand sequences are found in **Table S3**.

oxDNA Simulation Details

All oxDNA[3-7] simulations were run on the oxDNA.org[8] server. The complex structures were constructed using the "vhelix" plug in for Maya. The structures were then converted to oxDNA input files using TacoxDNA.[9] All structures were relaxed by checking the "needs relaxed" box in the simulation parameter settings. The average sequence model parameter was not used for any of the structures.

The smallest structures including external toehold complexes with zero, one, and two arms as well as internal toehold complexes with zero and one auxiliary arm all prompted errors when initially running. The errors read:

ERROR: A cell contains more than _max_n_per_cell (120) particles. Please increase the value of max_density_multiplier (which defaults to 1) in the input file

Since the input file cannot be altered while using the server and our local server was unavailable, we followed a suggestion on the oxDNA Source Forge discussion board which mentions shrinking the size of the box being used to avoid this problem. For these smallest complexes a box side length of 25 units was used instead of the size of 100 units used for all other structures.

oxDNA Input File Parameters

conf_file = MD_relax.dat
topology = output.top
mismatch_repulsion = 0
use_average_seq = 0
T = 25C
job_title = ET0
steps = 1000000000
salt_concentration = 1
backend = CUDA
interaction_type = DNA2
print_conf_interval = 500000
print_energy_every = 50000
dt = 0.001
external_forces = 0
sim_type = MD
max_density_multiplier = 10
verlet_skin = 0.5
time_scale = linear
ensemble = NVT
thermostat = john
diff_coeff = 2.5
backend_precision = mixed
lastconf_file = last_conf.dat
trajectory_file = trajectory.dat
energy_file = energy.dat
refresh_vel = 1
restart_step_counter = 1
newtonian_steps = 103
CUDA_list = verlet
CUDA_sort_every = 0
use_edge = 1
edge_n_forces = 1

oxDNA Simulation Images

Unconstrained External Toehold Complexes

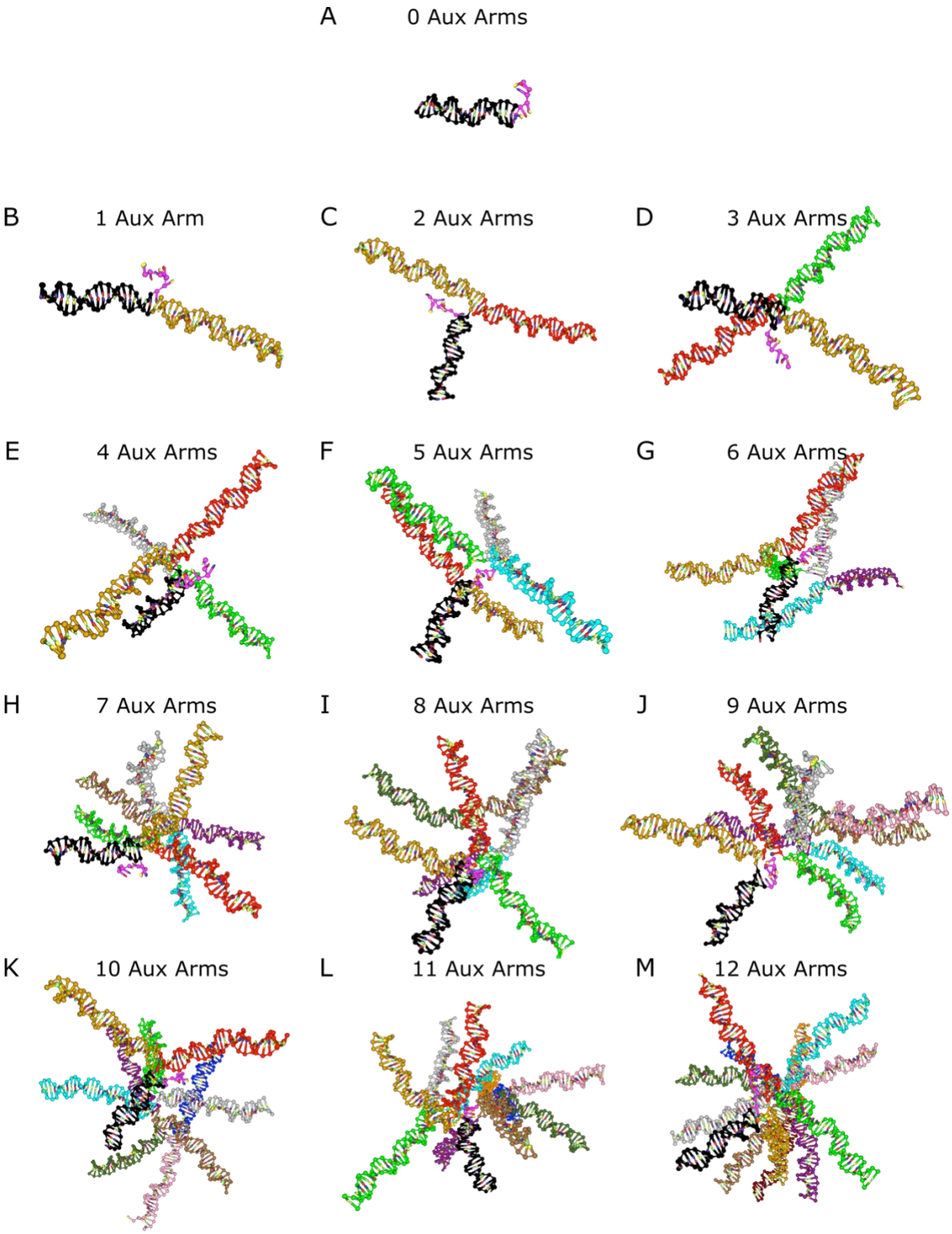

Figure S5 oxDNA simulation images of unconstrained external toehold complexes. **A**-**M** present complexes with 0-12 auxiliary arms respectively. Auxiliary arms retain colors close to those presented in schematic **Figure S2** with a hot pink toehold for better distinction.

Unconstrained Internal Toehold Complexes

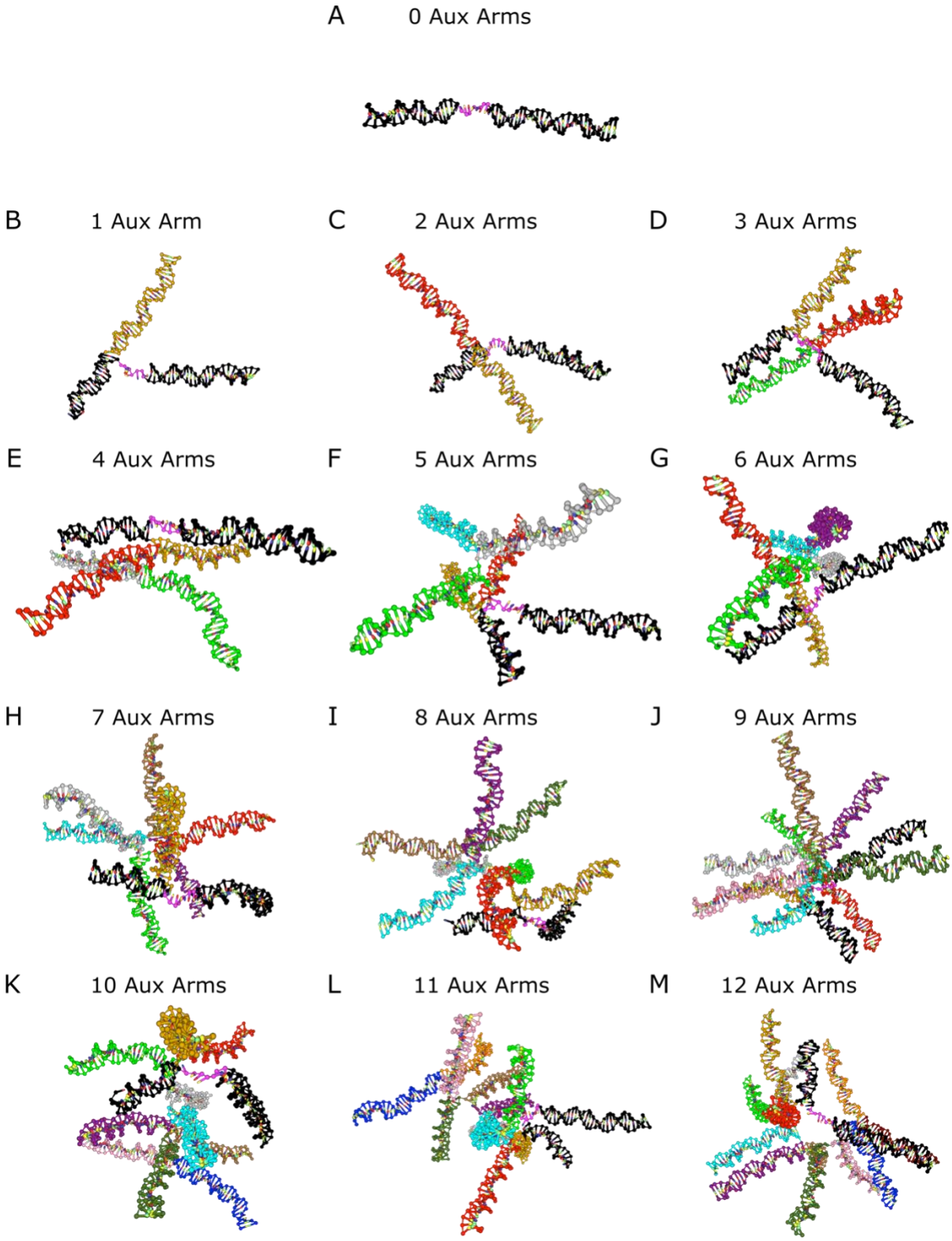

Figure S6 oxDNA simulation images of unconstrained internal toehold complexes. **A-M** present complexes with 0-12 auxiliary arms respectively. Auxiliary arms retain colors close to those presented in schematic **Figure S3** with a hot pink toehold for better distinction.

Constrained Toehold Complexes

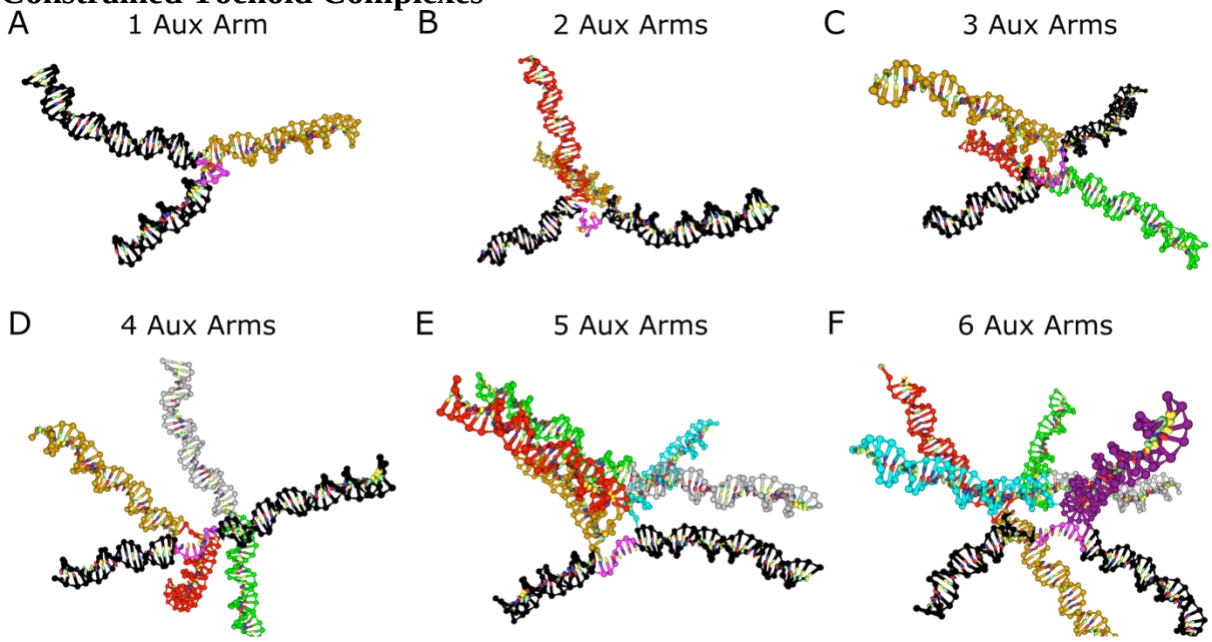

Figure S7 oxDNA simulation images of constrained toehold complexes. **A-F** present complexes with 1-6 auxiliary arms respectively. Auxiliary arms retain colors close to those presented in schematic **Figure S4** with a hot pink toehold for better distinction.

oxDNA Simulation Data: Average number of Nucleotides within Varying Radii

Unconstrained External Toehold Complexes

Table S4 Average number of nucleotides within varying radial distances from the middle nucleotide (4th) of the reporter toehold for oxDNA simulated external toehold complexes. Complexes are labeled with "ETX" where ET represents "external toehold unconstrained complex", and the X represents the number of arms of that complex.

Radius (nm)	ET0 (nt)	ET1 (nt)	ET2 (nt)	ET3 (nt)	ET4 (nt)	ET5 (nt)	ET6 (nt)	ET7 (nt)	ET8 (nt)	ET9 (nt)	ET10 (nt)	ET11 (nt)	ET12 (nt)
1	4.8	4.8	4.9	4.9	4.9	4.8	4.9	4.8	4.8	4.8	4.9	4.9	4.8
2	19.2	20.4	16.7	16.7	16.7	20.9	16.8	21.1	16.8	21.0	16.8	16.8	21.5
3	28.6	36.7	23.1	23.2	23.3	43.2	23.6	44.1	23.9	43.9	24.3	24.3	41.7
4	36.1	52.1	29.3	29.7	30.2	81.0	31.4	83.5	32.4	84.5	33.7	33.8	80.4
5	42.4	65.6	35.7	36.9	38.2	125.1	41.5	131.3	44.0	135.1	46.8	46.7	129.8
6	46.0	78.2	42.5	45.5	48.5	171.5	54.9	187.6	60.2	195.3	64.9	64.7	189.7
7	46.0	90.4	50.2	56.5	62.3	215.4	73.3	247.9	82.6	262.9	89.5	89.7	259.1
8	46.0	100.7	59.9	71.5	81.3	255.6	99.1	307.0	113.3	334.2	123.5	123.8	336.1
9	46.0	105.8	73.9	91.5	107.1	290.4	133.1	359.9	152.9	403.5	168.2	168.7	412.6
10	46.0	106.0	91.3	115.6	137.9	315.5	173.5	400.4	200.8	461.9	223.1	223.9	487.6
11	46.0	106.0	106.9	139.7	168.7	333.5	215.7	430.7	253.2	508.4	282.9	285.7	558.5
12	46.0	106.0	119.2	160.0	195.2	341.5	255.7	448.1	304.6	539.5	341.9	349.0	618.5
13	46.0	106.0	129.5	176.6	217.4	344.7	291.6	457.7	353.1	559.9	399.4	411.1	664.7
14	46.0	106.0	138.4	190.3	236.0	345.7	322.5	462.7	396.3	572.6	452.8	469.9	699.5
15	46.0	106.0	146.3	201.7	251.5	346.0	348.3	464.9	433.5	579.9	501.7	524.8	724.4
16	46.0	106.0	153.3	211.2	264.5	346.0	369.4	465.7	464.4	583.6	544.3	574.5	741.5
17	46.0	106.0	159.4	218.7	274.8	346.0	385.8	465.9	489.1	585.2	579.3	616.6	752.4
18	46.0	106.0	164.1	223.9	282.3	346.0	397.4	466.0	507.1	585.8	605.9	649.5	759.2
19	46.0	106.0	166.0	225.9	285.5	346.0	403.3	466.0	517.5	586.0	623.3	672.0	763.0
20	46.0	106.0	166.0	226.0	285.9	346.0	405.1	466.0	522.2	586.0	633.4	685.9	764.8
20+	0.0	0.0	0.0	0.0	0.1	0.0	0.9	0.0	3.8	0.0	12.6	20.1	1.2

Unconstrained Internal Toehold Complexes

Table S5 Average number of nucleotides within varying radial distances from the middle nucleotide (4th) of the reporter toehold for oxDNA simulated internal toehold complexes. Complexes are labeled with "ITX" where IT represents "internal toehold unconstrained complex", and the X represents the number of arms of that complex.

Radius (nm)	IT0 (nt)	IT1 (nt)	IT2 (nt)	IT3 (nt)	IT4 (nt)	IT5 (nt)	IT6 (nt)	IT7 (nt)	IT8 (nt)	IT9 (nt)	IT10 (nt)	IT11 (nt)	IT12 (nt)
1	4.8	4.8	4.9	4.9	4.9	4.8	4.9	4.8	4.8	4.8	4.8	4.9	4.9
2	19.3	20.6	16.7	16.7	16.7	21.1	16.8	21.1	16.8	21.1	16.8	16.8	21.2
3	29.8	37.8	23.3	23.3	23.5	43.8	23.9	43.9	24.1	44.1	24.3	24.4	43.6
4	42.0	56.8	29.8	30.3	30.7	82.9	32.1	83.9	33.1	84.6	34.1	34.0	83.6
5	55.7	76.8	36.9	38.5	39.8	129.1	43.0	132.8	45.5	135.0	47.2	47.4	134.1
6	66.3	96.8	45.4	48.6	51.7	178.9	58.1	191.6	62.4	195.8	65.7	66.3	195.9
7	73.0	115.9	55.9	61.9	67.8	228.2	79.0	255.3	85.6	265.2	91.3	92.9	267.6
8	79.6	133.1	69.2	79.5	90.0	275.2	107.4	318.9	117.6	339.8	125.8	128.5	347.4
9	86.1	144.9	87.7	103.7	120.1	317.0	145.1	377.5	159.5	413.3	172.2	175.2	430.4
10	92.8	151.8	110.6	133.0	156.2	349.1	189.3	424.6	209.8	476.7	228.9	233.2	509.4
11	99.4	158.5	132.6	161.7	191.9	373.2	235.3	461.8	265.2	529.5	289.9	297.9	582.4
12	103.7	163.1	151.3	187.1	223.7	386.7	279.7	485.9	320.2	567.4	351.4	364.5	643.2
13	105.7	165.2	167.6	209.4	251.6	394.6	320.1	501.3	372.6	594.4	412.1	429.9	692.7
14	106.0	165.9	181.6	228.5	275.4	399.5	356.0	511.2	420.6	613.0	470.5	492.3	731.6
15	106.0	166.0	193.7	244.9	295.7	402.7	386.8	517.5	462.7	625.5	524.2	550.3	761.0
16	106.0	166.0	204.3	258.9	312.8	404.6	412.4	521.3	499.1	633.7	572.3	603.2	782.3
17	106.0	166.0	213.3	270.2	326.6	405.5	433.0	523.7	528.9	638.9	613.3	649.2	797.3
18	106.0	166.0	220.3	278.6	336.7	405.9	448.2	525.0	551.6	642.0	645.5	686.5	807.7
19	106.0	166.0	223.9	282.9	342.0	406.0	456.9	525.6	565.9	643.9	667.7	713.7	814.6
20	106.0	166.0	225.1	284.4	343.9	406.0	461.1	525.9	573.9	645.0	681.6	731.7	819.3
20+	0.0	0.0	0.9	1.6	2.1	0.0	4.9	0.1	12.1	1.0	24.4	34.3	6.7

Constrained Toehold Complexes

Table S6 Average number of nucleotides within varying radial distances from the middle nucleotide (4th) of the reporter toehold for oxDNA simulated constrained toehold complexes. Complexes are labeled with "CCX" where CC represents "constrained complex", and the X represents the number of arms of that complex.

Radius (nm)	CC1 (nt)	CC2 (nt)	CC3 (nt)	CC4 (nt)	CC5 (nt)	CC6 (nt)
1	5.0	4.9	4.9	4.8	4.9	4.8
2	23.8	22.8	23.4	22.8	23.6	23.5
3	47.2	50.4	54.3	53.8	56.7	58.0
4	69.0	82.5	92.5	97.5	103.4	107.6
5	88.6	110.0	127.9	142.7	155.0	165.1
6	107.6	136.1	161.4	184.9	206.0	225.3
7	125.8	161.4	193.8	225.0	253.7	282.2
8	141.9	185.1	225.0	263.7	299.0	335.6
9	153.8	204.9	252.6	298.4	340.2	383.4
10	160.2	216.9	270.8	323.1	370.9	419.6
11	165.3	224.6	282.4	338.6	392.0	444.7
12	166.0	226.0	285.6	344.1	401.3	457.4
13	166.0	226.0	286.0	345.7	404.8	463.2
14	166.0	226.0	286.0	346.0	405.8	465.4
15	166.0	226.0	286.0	346.0	406.0	465.9
16	166.0	226.0	286.0	346.0	406.0	466.0
17	166.0	226.0	286.0	346.0	406.0	466.0
18	166.0	226.0	286.0	346.0	406.0	466.0
19	166.0	226.0	286.0	346.0	406.0	466.0
20	166.0	226.0	286.0	346.0	406.0	466.0

oxDNA Simulation Experimental Data Correlation

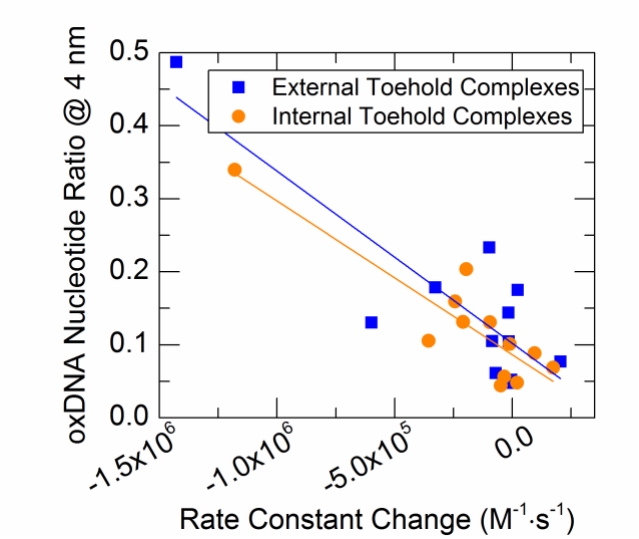

Figure S8 Experimental rate constant changes are plotted against oxDNA nucleotide ratios to determine a correlation. Pearson correlation coefficients of -0.85 and -0.89 were found for external and internal complexes respectively.

Unconstrained Internal Toehold Complexes Vs. Constrained Toehold Complexes

oxDNA was used to model structures from both the unconstrained and constrained subsets of complexes. Models of the unconstrained internal toehold complexes and constrained complexes with auxiliary arms from one to six were particularly important so that the increased steric hindrance that a constrained complex provides could be compared. Internal toehold complexes are shown in **Figure S9,** and constrained complexes are shown in **Figure S10**.

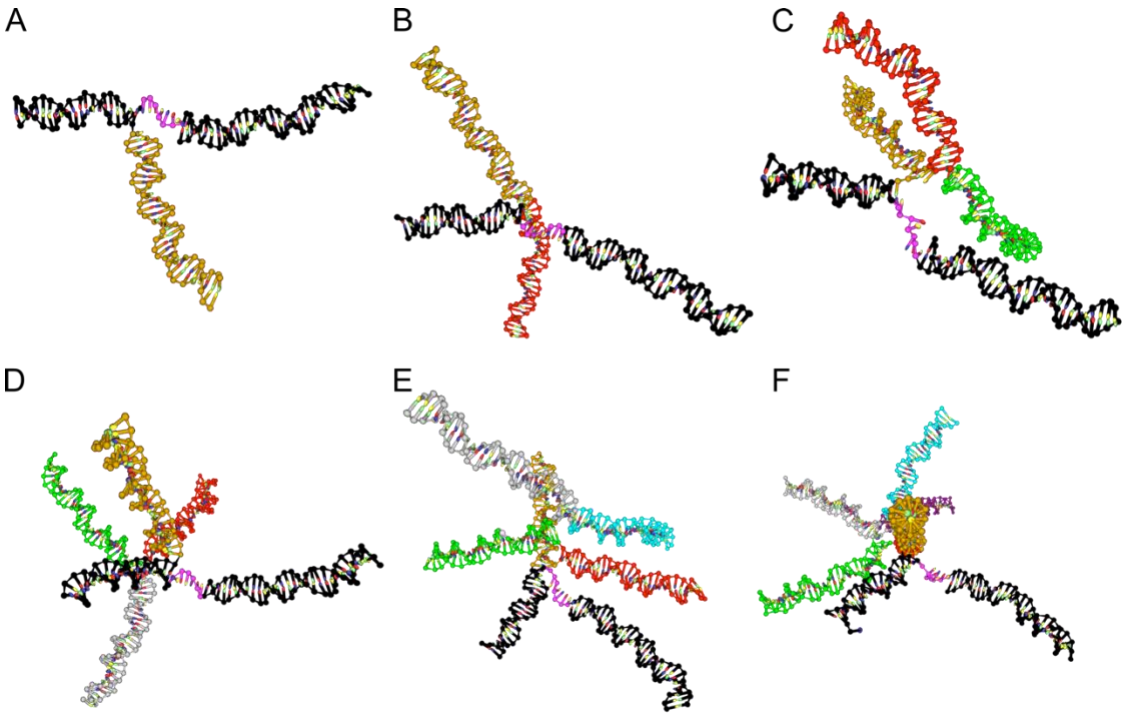

Figure S9 Unconstrained internal toehold complexes modeled using oxDNA. Structures with 1-6 auxiliary arms are shown in **A-F** respectively. The structures are all oriented similarly relative reporter complex. The short (20 bp) black duplex shown on left side of each image represents the reporter duplex. The pink 7 nt single stranded portion shown near the middle of the images is the toehold. The longer (30 bp) black duplex is the extra duplex on the opposite side of the toehold to make the toehold "internal" as discussed in the main text of the manuscript. The auxiliary arms are color coded to match the schematics in **Figure S3** as well as the strand sequences given in **Table S1**. The first through the sixth arms are colored in gold, red, green, silver, blue, and purple respectively.

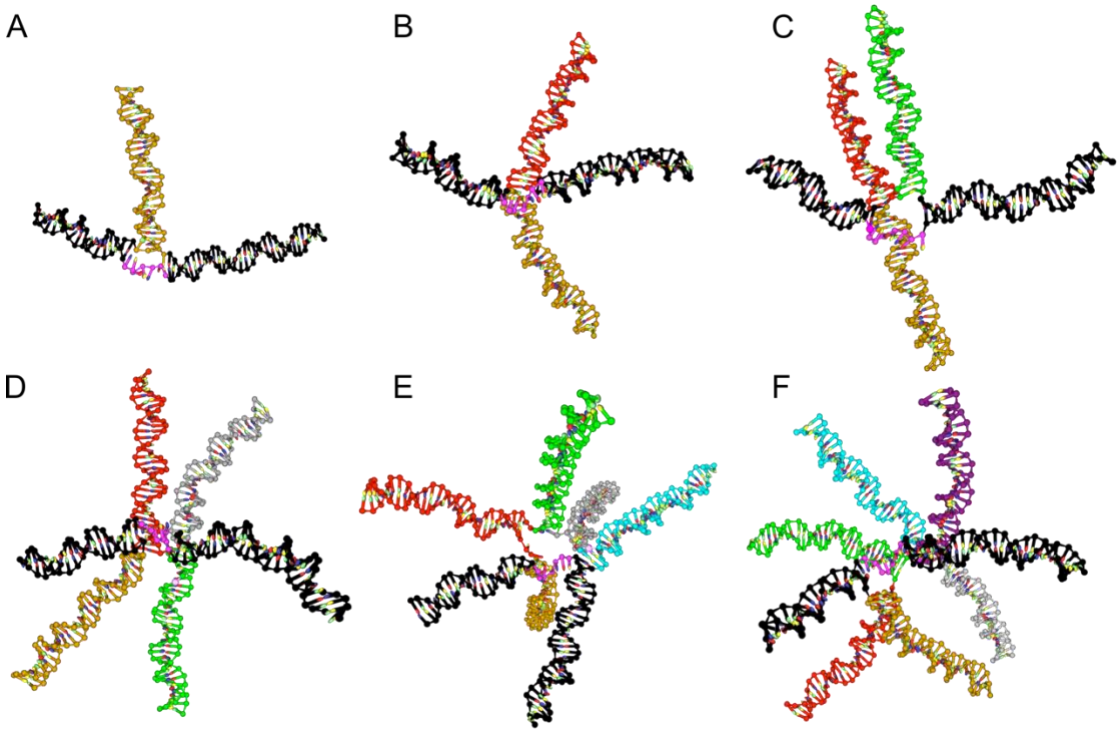

Figure S10 oxDNA modeled constrained toehold complexes. Structures with 1-6 auxiliary arms are shown in **A-F** respectively. The structures are all oriented similarly relative to the reporter complex. The short (20 bp) black duplex shown on left side of each image represents the reporter complex. The pink 7 nt single stranded portion shown near the middle of the images is the toehold. Similar to the internal toehold complexes, constrained complexes possess a longer (30 bp) black duplex on the opposite side of the toehold. This duplex is shown in black on the right side of the toehold in each of these images. The auxiliary arms are color coded to match the schematics in **Figure S4** as well as the strand sequences given in **Table S1** and **S3**. The first through the sixth arms are colored in gold, red, green, silver, blue, and purple respectively.

After running simulations in oxDNA, the trajectory files were used to determine the average number of nucleotides within varying radius distances from the middle nucleotide of the toehold. The average number of nucleotides was then divided by spherical volume associated with each radius to give the spherical density in units of nt/nm^3 for each structure. Spherical densities were compared between the unconstrained internal toehold complexes and constrained complexes. percentage of constrained to unconstrained spherical densities is given in **Table S7**.

Table S7 Percent increase of nucleotide density from unconstrained internal toehold complex to constrained complexes.

% Density (nt/nm^3) Increase from Unconstrained Internal Toehold to Constrained Toehold Complexes

Radius (nm)	1 Aux. Arm	2 Aux. Arms	3 Aux. Arms	4 Aux. Arms	5 Aux. Arms	6 Aux. Arms
1	3.50	0.70	0.42	-1.59	1.22	-0.87
2	15.71	36.42	40.03	36.41	11.94	39.94
3	24.76	116.48	132.92	129.59	29.38	142.95
4	21.58	177.17	205.50	217.30	24.74	234.87
5	15.37	198.07	232.38	258.60	20.09	284.07
6	11.25	200.08	232.09	257.78	15.11	287.69
7	8.53	188.99	213.26	232.04	11.15	257.33
8	6.66	167.57	183.14	192.97	8.66	212.46
9	6.13	133.71	143.66	148.41	7.31	164.27
10	5.52	96.01	103.58	106.87	6.24	121.64

At a one nanometer radius there is negligible differences between the nucleotide densities. Since the width of the typical DNA duplex is about two nanometers, the spherical density at one nanometer would not be expected to change much between the unconstrained and constrained and thus, these values are disregarded. As the radius is increased from two to ten nanometers, the spherical density increases dramatically from unconstrained complexes to constrained complexes with the same number of arms and thus the same exact sequences and number of nucleotides. This result is expected due to the extra attachment point helping concentrate the steric auxiliary arms closer to the toehold. More highly concentrated nucleotides provide more steric hindrance that an invasion strand must fight in order to access the toehold and thus kinetics are expected to slow as shown in the data from **Figure 4** of the manuscript.

Python Script for oxDNA Simulation Nucleotide Distance Calculator

```
import numpy as np
import time
startTime = time.time()

maxradius = 20
toeholdpos = 24
counted = np.empty(0)
averages = []
countersize = maxradius+1

rawfile = open('file.dat', 'r')
datafile = rawfile.read()
rawfile.close()

datapods = datafile.split('t = ')
datapods.pop(0)

for data in datapods:
    data = data.split('\n')
    data.pop(-1)

    l = data[1]
    box = l.split(' ')
    box = np.array(box[2:], dtype=float)

    data = data[3:]
    array = np.genfromtxt(data, dtype=float)
    newArray = array[:, 0:3]

    counterarray = np.array([0]*countersize)

    for element in newArray:

        p1 = element
        p2 = newArray[len(newArray)-toeholdpos]

        p1 = p1 - (np.floor(p1/box) * box)
        p2 = p2 - (np.floor(p2/box) * box)
        diff = p1 - p2
        diff = diff - (np.round(diff/box) * box)
        distance = (np.linalg.norm(diff)) * 0.85

        for radius in range(1, maxradius + 1):
            if 0 < distance < radius:
                counterarray[radius-1] = counterarray[radius-1] + 1
        if distance >= maxradius:
            counterarray[maxradius] = counterarray[maxradius]+1

    counted = np.concatenate((counted, counterarray),axis=0)

counted = np.reshape(counted, (-1, countersize)).T

for rArray in counted:
    average = sum(rArray)/len(rArray)
    averages.append(average)

averages = np.reshape(averages, (countersize, 1))

print(str(averages).replace(' [', '').replace('[', '').replace(']', ''))

executionTime = (time.time()-startTime)
print('Execution time in seconds: '+str(executionTime))
```

Kinetics Curves

Unconstrained External Toehold Complexes

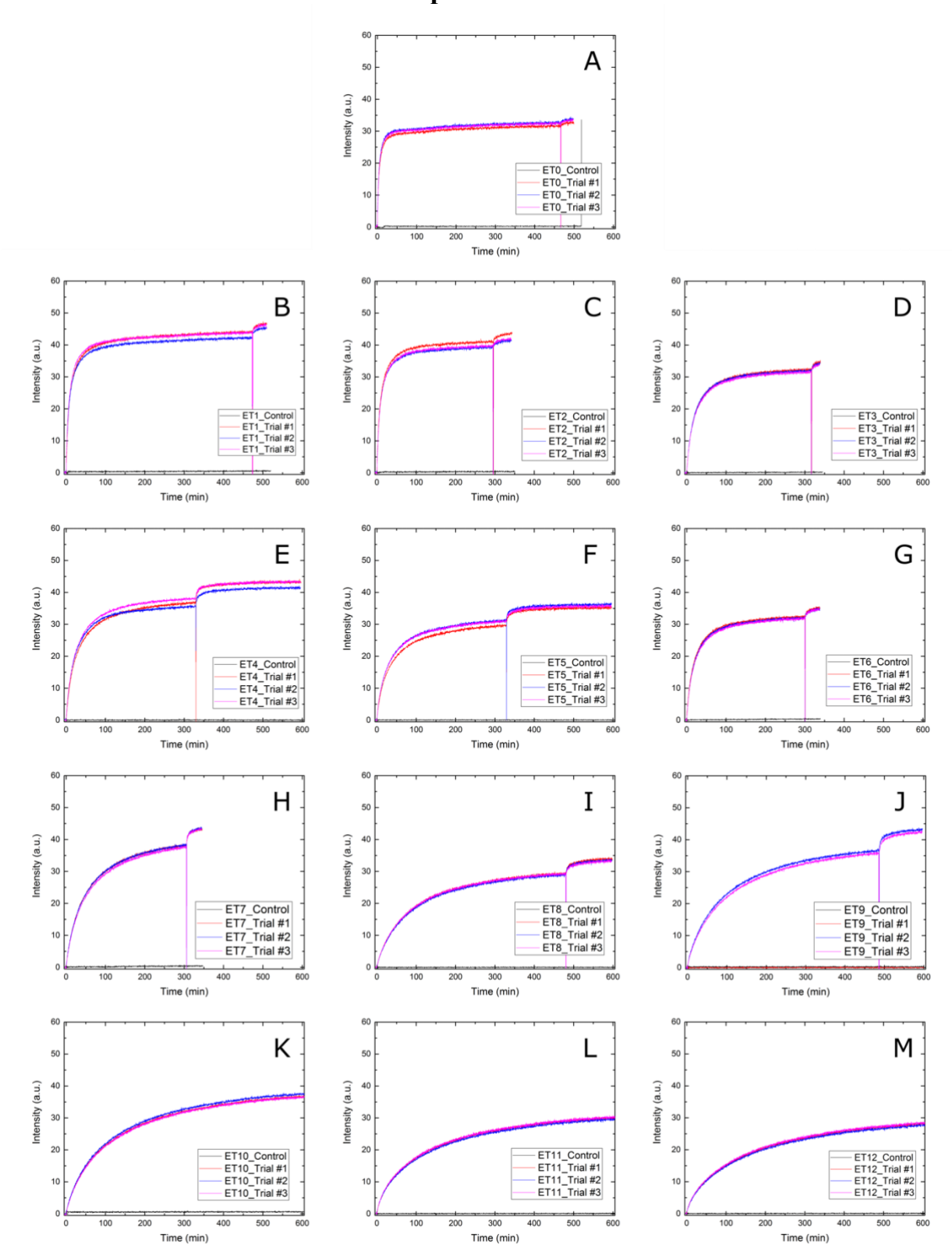

Figure S11 Unconstrained external toehold complex kinetics curves. **A-M** present raw kinetics data from external toehold complexes with 0-12 auxiliary arms respectively.

Unconstrained Internal Toehold Complexes

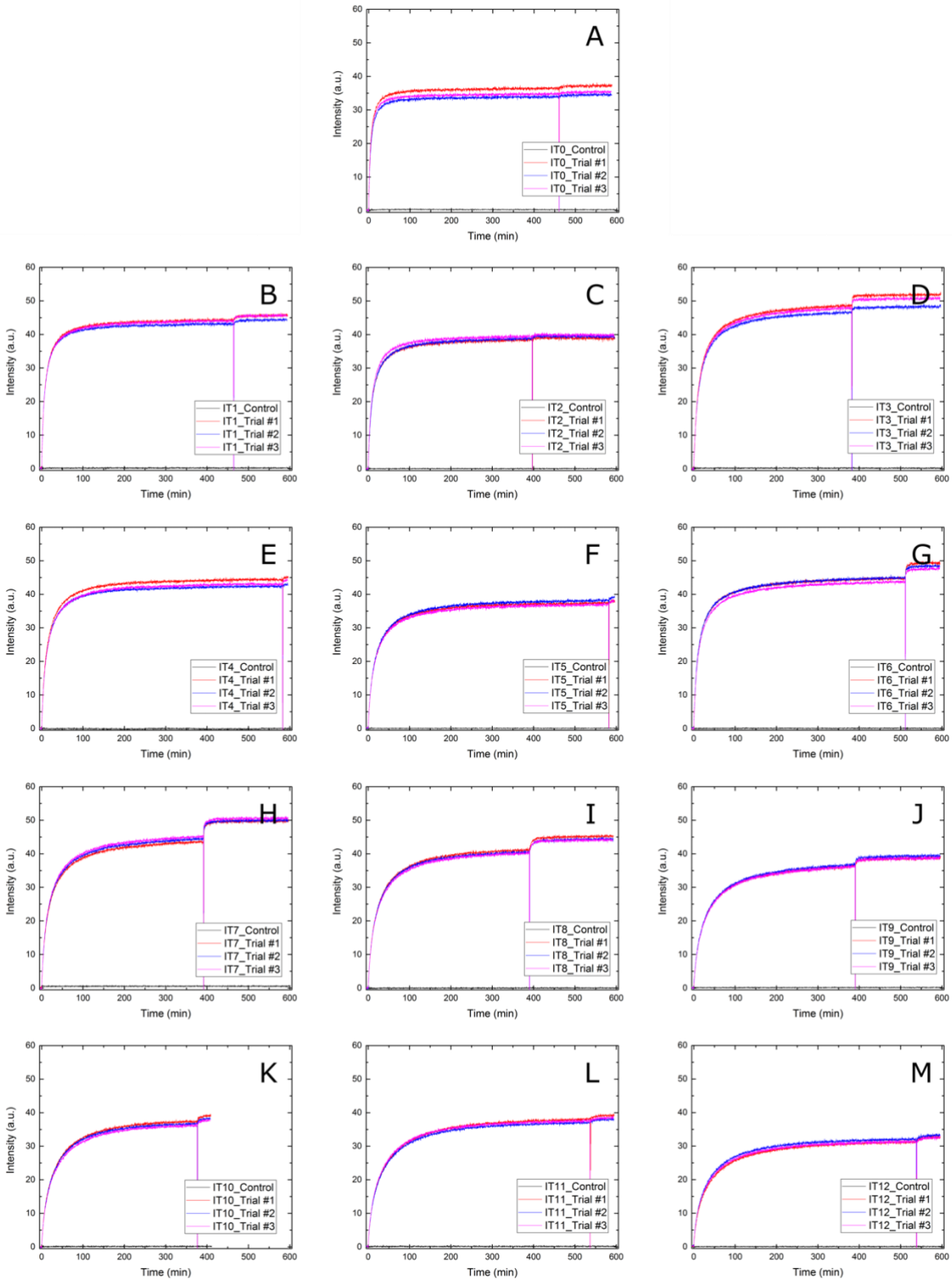

Figure S12 Unconstrained internal toehold complex kinetics curves. **A-M** present raw kinetics data from internal toehold complexes with 0-12 auxiliary arms respectively.

Constrained Complexes

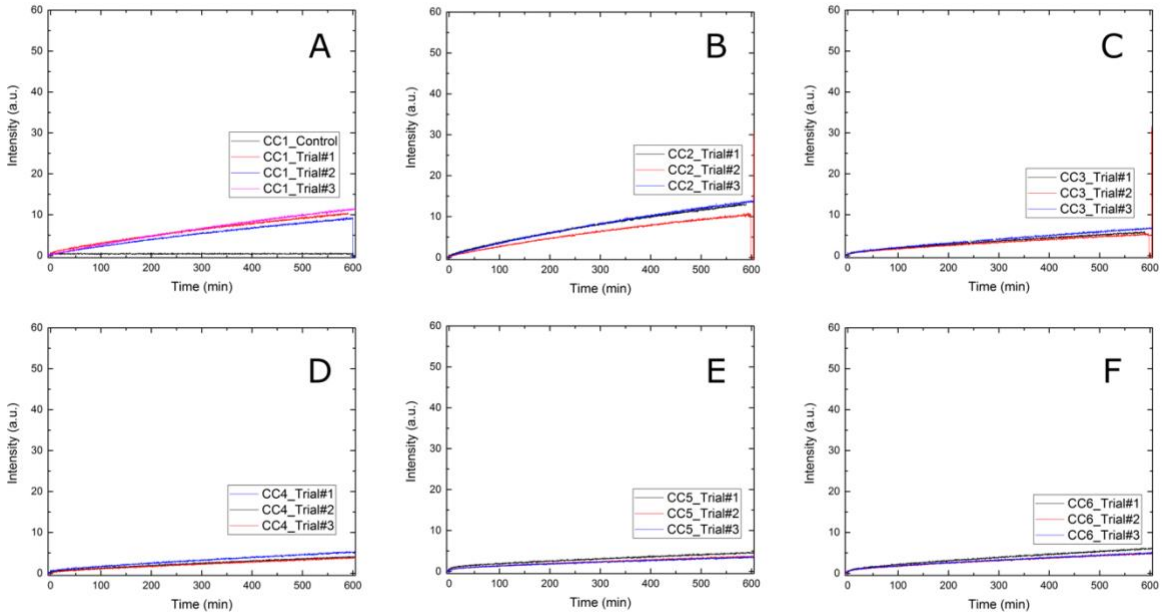

Figure S13 Constrained complex kinetics curves. **A-F** present raw kinetics data from constrained complexes with 1-6 auxiliary arms.

Unconstrained External Toehold Complexes with Truncated Auxiliary Arms

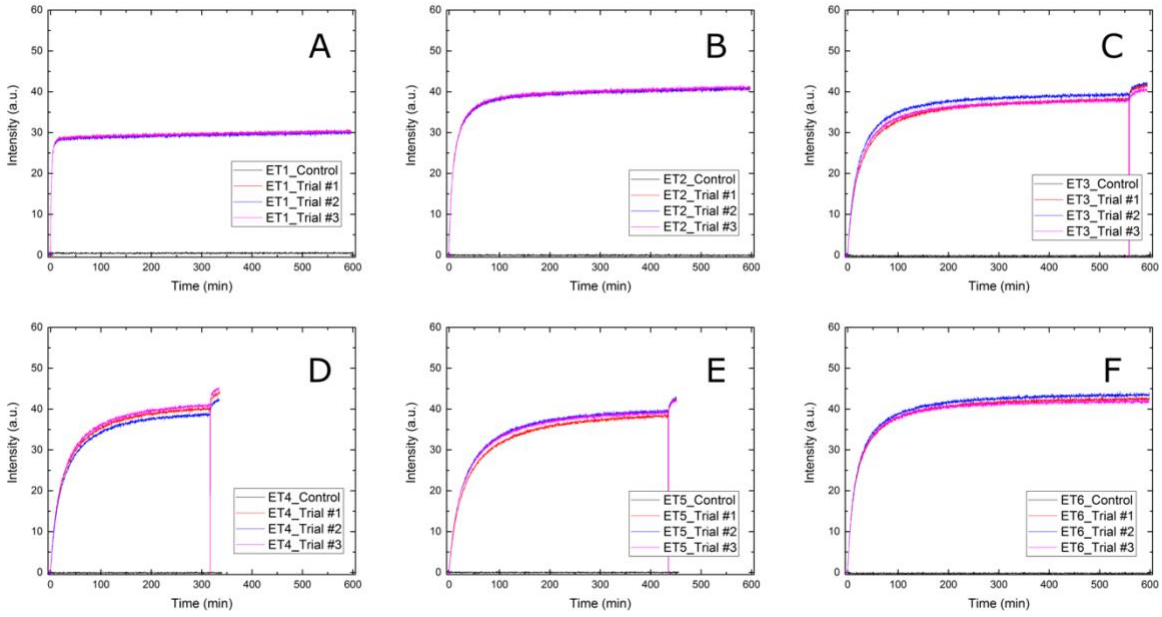

Figure S14 Unconstrained external toehold complexes with truncated auxiliary arms (from 30 bp to 20 bp) kinetics curves. **A-F** present raw kinetics data from unconstrained external toehold complexes with 1-6 auxiliary arms.

Unconstrained Internal Toehold Complexes with Truncated Auxiliary Arms

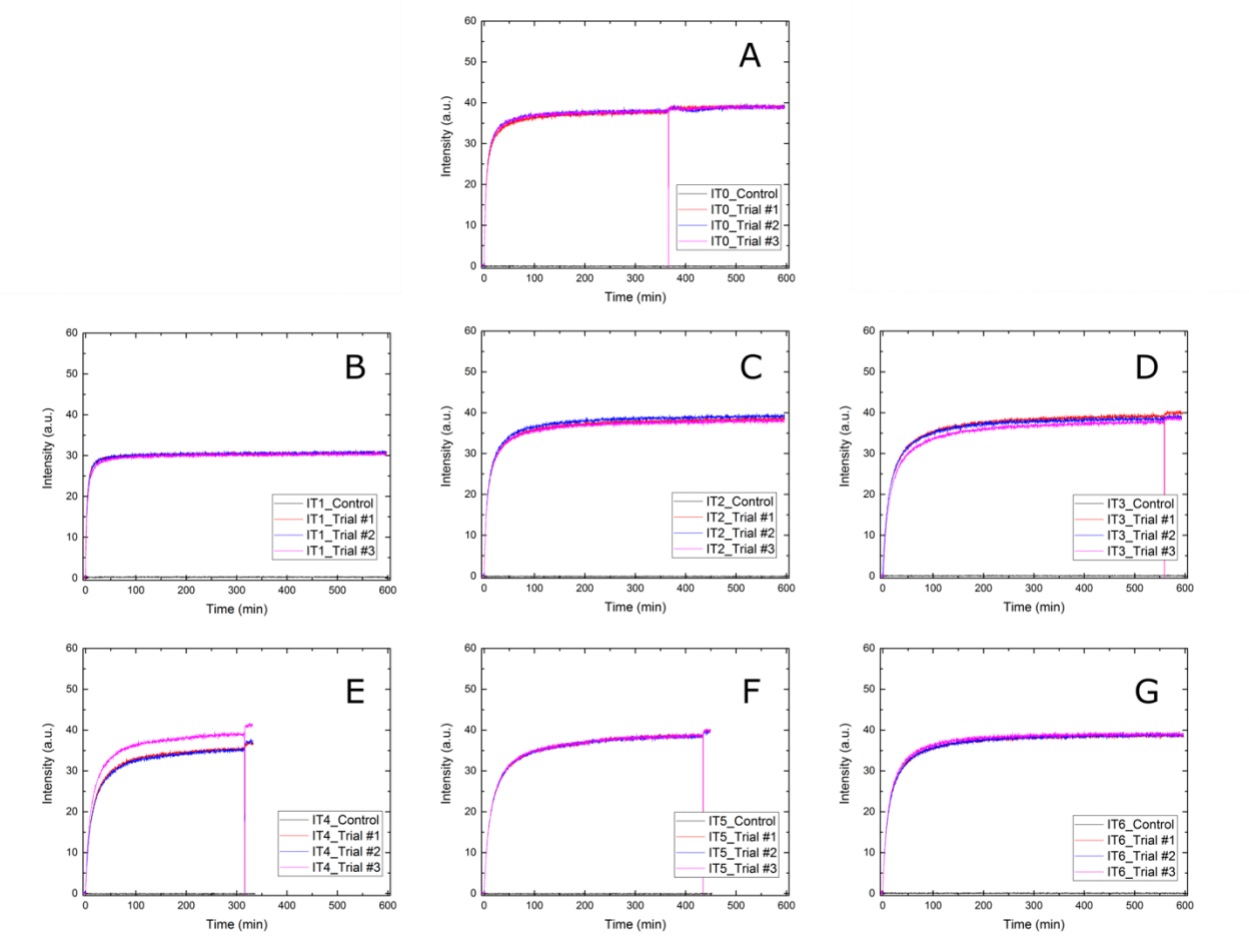

Figure S15 Unconstrained internal toehold complexes with truncated auxiliary arms (from 30 bp to 20 bp) kinetics curves. **A-G** present raw kinetics data from unconstrained internal toehold complexes with 0-6 auxiliary arms.

Low Salt External Toehold Kinetics Curves

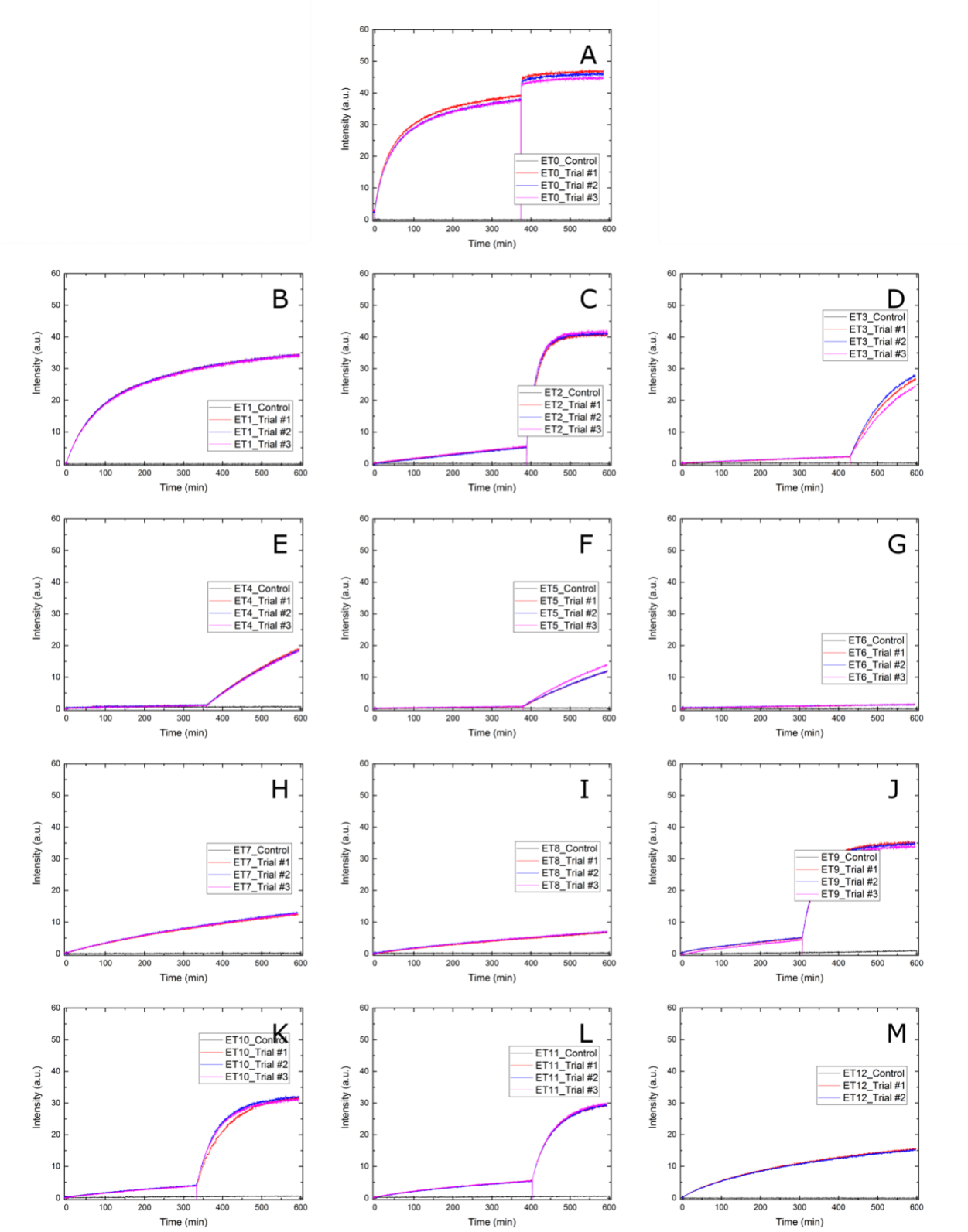

Figure S16 Unconstrained external toehold complex kinetics curves in 1.25 mM $MgCl_2$. **A-M** present raw kinetics data from external toehold complexes with 0-12 auxiliary arms respectively.

Low Salt Internal Toehold Kinetics Curves

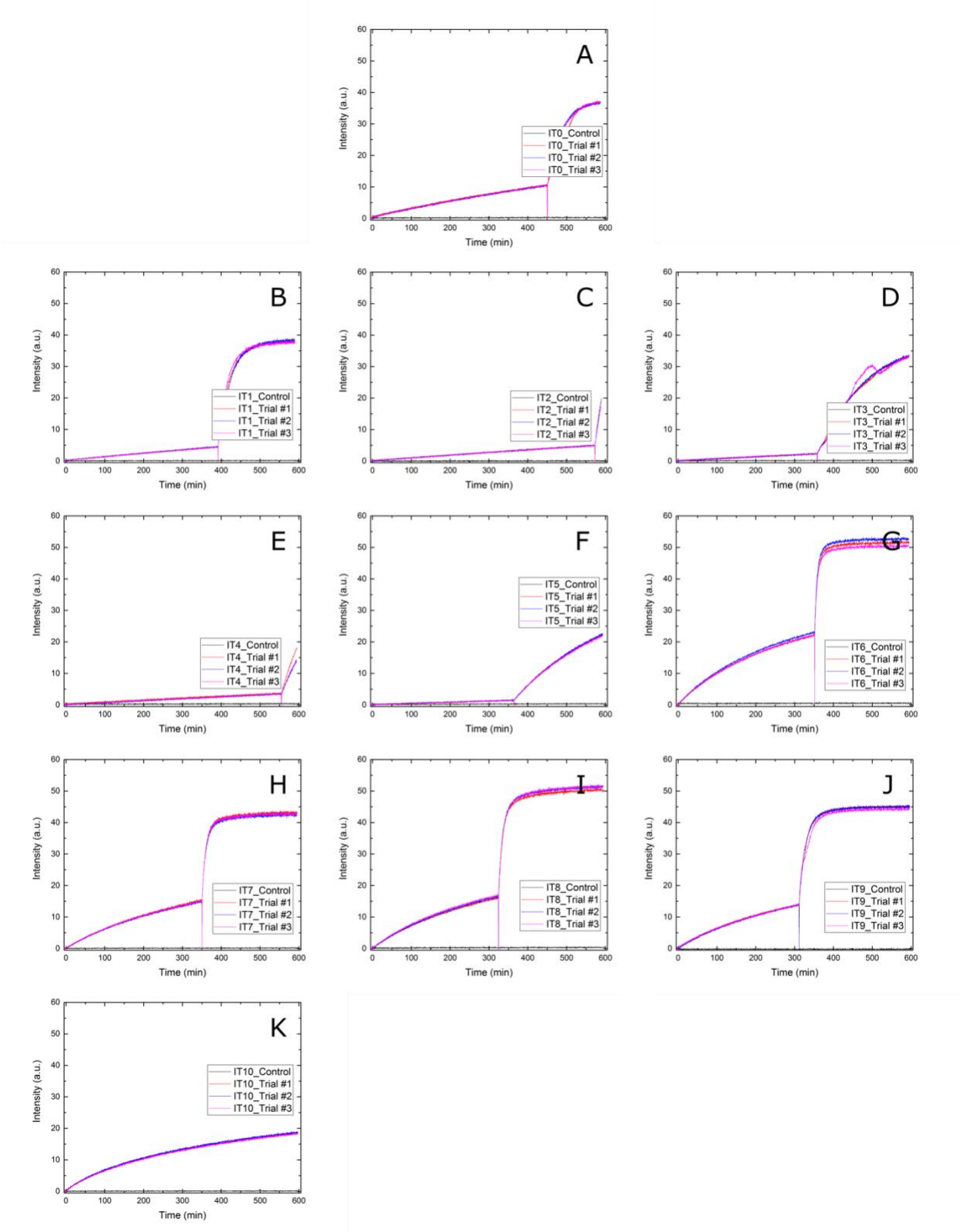

Figure S17 Unconstrained internal toehold complex kinetics curves in 1.25 mM $MgCl_2$. **A-K** present raw kinetics data from external toehold complexes with 0-12 auxiliary arms respectively.

High Salt External Toehold Kinetics Curves

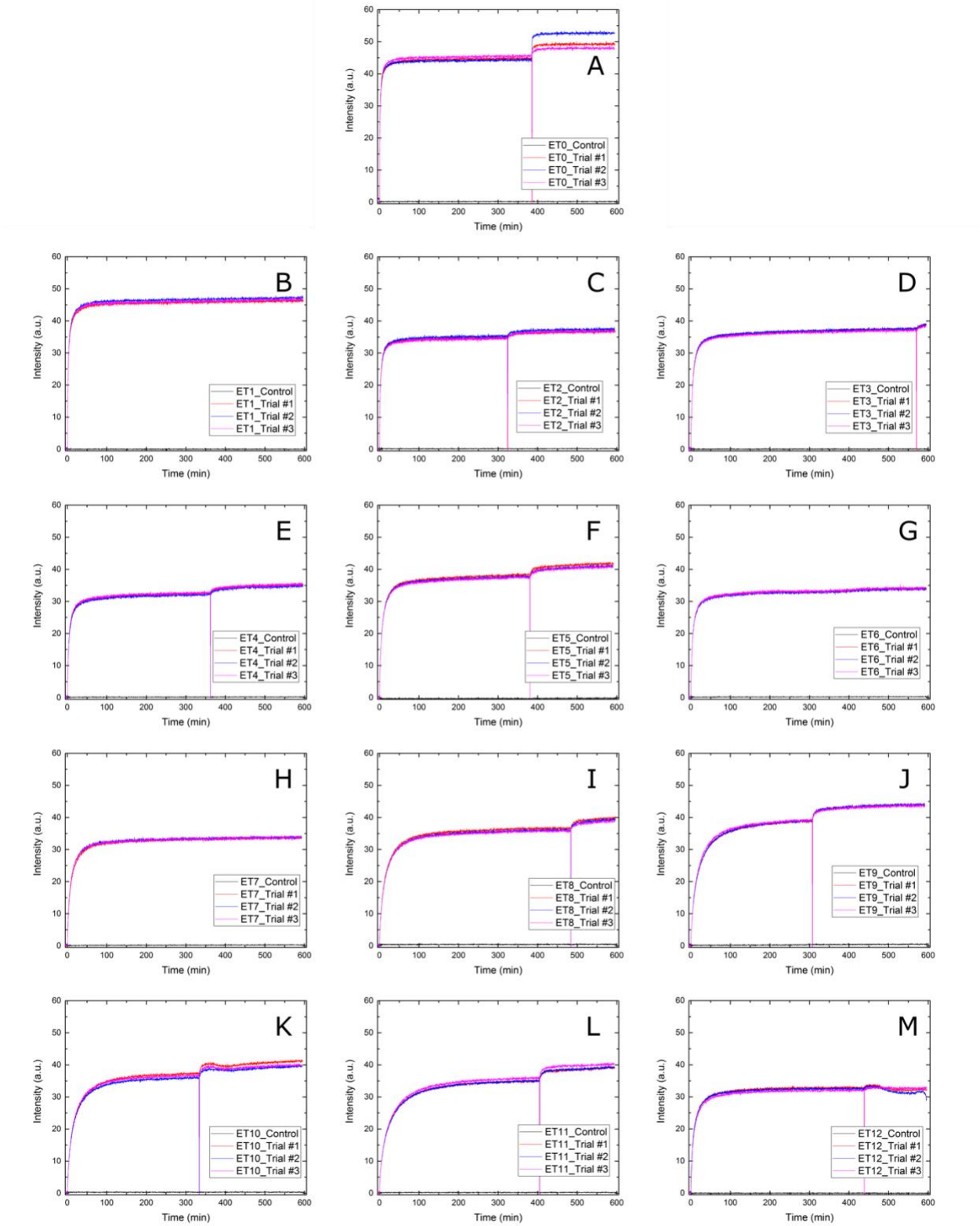

Figure S18 Unconstrained external toehold complex kinetics curves in 125 mM $MgCl_2$. **A-M** present raw kinetics data from external toehold complexes with 0-12 auxiliary arms respectively.

High Salt Internal Toehold Kinetics Curves

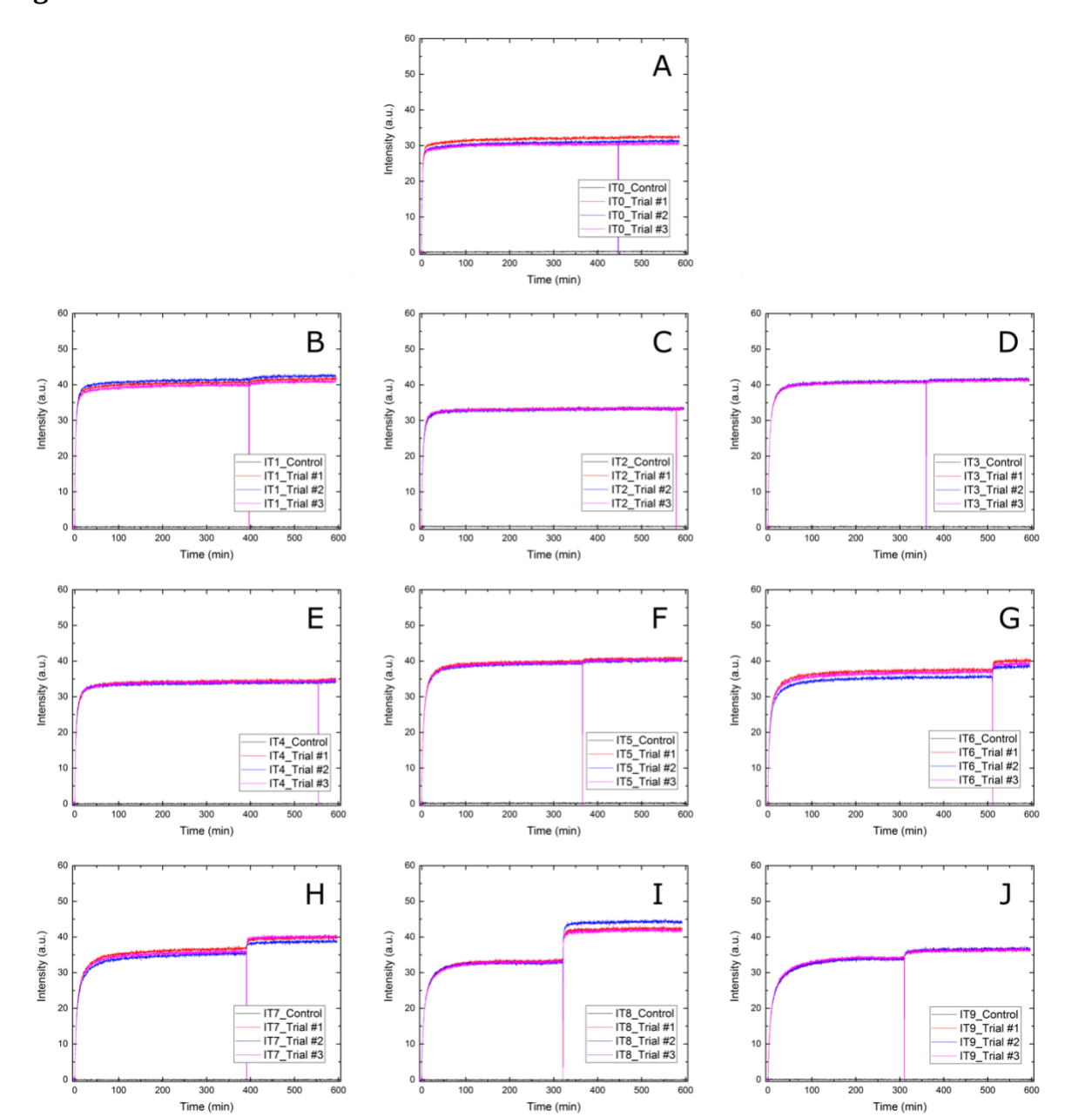

Figure S19 Unconstrained internal toehold complex kinetics curves in 125 mM $MgCl_2$. **A-J** present raw kinetics data from external toehold complexes with 0-12 auxiliary arms respectively.

Kinetics Experiment Details

For each experimental complex three technical replicates and a control curve were collected. Control curves present the monitoring of complexes with no invader for the duration of the experiment. This ensures that the complexes are not spontaneously dissociating.
All kinetics curves were run at least 300 minutes while most were run 600+ minutes. After 300 minutes vertical portions of the curves are observed in some experimental runs. These points indicate where the cuvettes were removed from the instrument and ~2 uL of ~100 uM concentrated invader was introduced to the cuvette to ensure that experiments were all finishing

at the same intensity. Ensuring experiments were finishing at the same intensity was needed to determine that concentrations weren't somehow being miscalculated and the observed trend of lower reaction rate constants with increasing complex size wasn't an artifact of incrementally over-estimating the concentrations with incremental complex growth. Since all max intensities (after the flood of invader) are roughly equal, we can assume that this problem did not occur and have more confidence in the results.

All curves are raw data curves shifted only along the x-axis so that the experiments, that are all started at slightly different times, can be compared from the start of each different cuvette's introduction of invader strands. As mentioned in the materials and methods section, these experiments were run on two of the (for all intents and purposes) same fluorescence spectrophotometers. While all the settings are the same (temperature, slit widths, excitation and emission wavelengths) there are slight differences in the maximum intensities of the same sample between the instruments. One instrument has a max intensity of around 35 a.u. at 2 nM concentrations while the other instrument has a maximum intensity of about 45 a.u. at the same concentrations. Besides the differences in max intensity between instruments, there do not look to be large enough differences between the max intensities to discourage confidence in the results.

Tabulated Rate Constant Data

Table S8 Rate constant and standard error data copied from Origin Lab fitting of kinetics traces shown in **Figure S11** of external toehold complexes in default (12.5 mM) $MgCl_2$ concentrations. Standard deviations were calculated via excel after copying and pasting data from Origin. External toehold complexes are represented by codes of the form ETx, where x is the number of auxiliary arms of the complex.

	Trial #1 ($M^{-1}s^{-1}$)		Trial #2 ($M^{-1}s^{-1}$)		Trial #3 ($M^{-1}s^{-1}$)		Average ($M^{-1}s^{-1}$)		
Complex	Rate Constant	St.Err.	Rate Constant	St.Err.	Rate Constant	St.Err.	Rate Constant	St.Err.	St.Dev.
ET0	2.35E+06	27055	2.57E+06	30839	2.53E+06	30121	2.48E+06	29338	120713
ET1	9.69E+05	4445	1.04E+06	5134	1.15E+06	5810	1.06E+06	5130	92991
ET2	1.03E+06	5644	1.11E+06	6755	1.09E+06	6451	1.08E+06	6283	40128
ET3	4.67E+05	2267	4.96E+05	2597	4.75E+05	2521	4.80E+05	2462	15201
ET4	3.96E+05	1923	4.00E+05	2031	3.85E+05	1837	3.94E+05	1930	7629
ET5	2.79E+05	1354	3.05E+05	1569	3.02E+05	1552	2.95E+05	1491	14499
ET6	5.10E+05	2765	5.09E+05	2816	4.80E+05	2547	5.00E+05	2709	17302
ET7	1.75E+05	651	1.74E+05	595	1.67E+05	607	1.72E+05	618	4315
ET8	1.01E+05	358	9.92E+04	354	1.03E+05	366	1.01E+05	359	1904
ET9	8.75E+04	271	8.22E+04	255	8.46E+04	229	8.48E+04	263	2626
ET10	8.01E+04	151	8.08E+04	152	7.93E+04	152	8.01E+04	152	757
ET11	7.33E+04	180	6.71E+04	164	7.11E+04	175	7.05E+04	173	3171
ET12	5.49E+04	130	5.54E+04	131	5.68E+04	134	5.57E+04	132	976

Table S9 Rate constant and standard error data copied from Origin Lab fitting of kinetics traces shown in **Figure S12** of internal toehold complexes in default (12.5 mM) $MgCl_2$ concentrations. Standard deviations were calculated via excel after copying and pasting data from Origin. External toehold complexes are represented by codes of the form ITx, where x is the number of auxiliary arms of the complex.

	Trial #1 ($M^{-1}s^{-1}$)		Trial #2 ($M^{-1}s^{-1}$)		Trial #3 ($M^{-1}s^{-1}$)		Average ($M^{-1}s^{-1}$)		
Complex	Rate Constant	St.Err.	Rate Constant	St.Err.	Rate Constant	St.Err.	Rate Constant	St.Err.	St.Dev.
IT0	2.30E+06	19732	2.33E+06	22259	2.47E+06	24248	2.37E+06	22080	93930
IT1	1.16E+06	5700	1.26E+06	6850	1.14E+06	5492	1.19E+06	6014	62023
IT2	8.78E+05	3925	1.06E+06	5596	9.95E+05	4888	9.79E+05	4803	93149
IT3	6.34E+05	3124	6.15E+05	3093	6.18E+05	3109	6.23E+05	3109	10071
IT4	7.12E+05	3162	7.54E+05	3908	6.85E+05	3083	7.17E+05	3384	35146
IT5	5.30E+05	2610	5.06E+05	2412	5.27E+05	2600	5.21E+05	2541	13159
IT6	6.34E+05	2820	7.01E+05	3650	7.50E+05	4185	6.95E+05	3551	58363
IT7	4.50E+05	2497	4.45E+05	2422	4.58E+05	2564	4.51E+05	2494	6677
IT8	4.12E+05	1745	4.31E+05	1795	4.07E+05	1692	4.17E+05	1744	12801
IT9	3.26E+05	1539	3.16E+05	1531	3.23E+05	1582	3.21E+05	1550	4917
IT10	3.38E+05	1515	3.52E+05	1590	3.34E+05	1504	3.41E+05	1536	9746
IT11	2.81E+05	1308	2.91E+05	1333	3.05E+05	1393	2.93E+05	1344	12084
IT12	2.70E+05	1523	2.90E+05	1612	2.86E+05	1564	2.82E+05	1566	10976

Table S10 Rate constant and standard error data copied from Origin Lab fitting of kinetics traces shown in **Figure S13** of constrained complexes in default (12.5 mM) $MgCl_2$ concentrations. Standard deviations were calculated via excel after copying and pasting data from Origin. Constrained complexes are represented by codes of the form CCx, where x is the number of auxiliary arms of the complex.

	Trial #1 ($M^{-1}s^{-1}$)		Trial #2 ($M^{-1}s^{-1}$)		Trial #3 ($M^{-1}s^{-1}$)		Average ($M^{-1}s^{-1}$)		
Complex	Rate Constant	St.Err.	Rate Constant	St.Err.	Rate Constant	St.Err.	Rate Constant	St.Err.	St.Dev.
CC1	5528	7	6180	7	5713	6	5807	7	336
CC2	6846	8	8109	10	7496	8	7483	9	632
CC3	2480	5	2419	5	2618	5	2506	5	102
CC4	1810	4	1717	4	1661	4	1729	4	75
CC5	1381	5	1438	5	1326	5	1382	5	56
CC6	2095	5	2030	6	2049	6	2058	5	34

Table S11 Rate constant and standard error data copied from Origin Lab fitting of kinetics traces shown in **Figure S14** of truncated external toehold complexes in default (12.5 mM) $MgCl_2$ concentrations. Standard deviations were calculated via excel after copying and pasting data from Origin. External toehold complexes are represented by codes of the form ETx, where x is the number of auxiliary arms of the complex.

	Trial #1 ($M^{-1}s^{-1}$)		Trial #2 ($M^{-1}s^{-1}$)		Trial #3 ($M^{-1}s^{-1}$)		Average ($M^{-1}s^{-1}$)		
Complex	Rate Constant	St.Err.	Rate Constant	St.Err.	Rate Constant	St.Err.	Rate Constant	St.Err.	St.Dev.
ET0	2.35E+06	27055	2.57E+06	30839	2.53E+06	30121	2.48E+06	29338	120713
ET1	1.08E+06	4682	1.14E+06	5263	1.20E+06	5829	1.14E+06	5258	57463
ET2	1.10E+06	5719	1.10E+06	5958	1.14E+06	6184	1.11E+06	5954	21369
ET3	4.02E+05	1563	4.75E+05	2136	4.66E+05	2092	4.48E+05	1930	39812
ET4	3.75E+05	1410	3.88E+05	1547	3.82E+05	1419	3.82E+05	1459	6070
ET5	2.73E+05	1004	3.04E+05	1090	3.00E+05	1097	2.92E+05	1064	16624
ET6	5.16E+05	2018	5.20E+05	1973	5.65E+05	2363	5.34E+05	2118	27162

Table S12 Rate constant and standard error data copied from Origin Lab fitting of kinetics traces shown in **Figure S15** of truncated internal toehold complexes in default (12.5 mM) $MgCl_2$ concentrations. Standard deviations were calculated via excel after copying and pasting data from Origin. External toehold complexes are represented by codes of the form ITx, where x is the number of auxiliary arms of the complex.

	Trial #1 ($M^{-1}s^{-1}$)		Trial #2 ($M^{-1}s^{-1}$)		Trial #3 ($M^{-1}s^{-1}$)		Average ($M^{-1}s^{-1}$)		
Complex	Rate Constant	St.Err.	Rate Constant	St.Err.	Rate Constant	St.Err.	Rate Constant	St.Err.	St.Dev.
IT0	1.87E+06	14514	2.15E+06	16018	2.10E+06	14714	2.04E+06	15082	148806
IT1	1.06E+06	6094	1.14E+06	6585	1.22E+06	7590	1.14E+06	6756	79343
IT2	1.04E+06	6950	1.05E+06	6843	1.07E+06	6599	1.05E+06	6797	17786
IT3	6.23E+05	3057	6.58E+05	3416	6.27E+05	3237	6.36E+05	3237	18926
IT4	7.16E+05	3804	6.79E+05	3721	7.68E+05	4116	7.21E+05	3880	44346
IT5	6.07E+05	3172	6.10E+05	3116	6.13E+05	3134	6.10E+05	3140	2941
IT6	7.16E+05	3658	7.14E+05	3614	7.73E+05	4100	7.34E+05	3790	33082

Table S13 Rate constant and standard error data copied from Origin Lab fitting of kinetics traces shown in **Figure S16** of external toehold complexes in low (1.25 mM) $MgCl_2$ concentrations. Standard deviations were calculated via excel after copying and pasting data from Origin. External toehold complexes are represented by codes of the form ETx, where x is the number of auxiliary arms of the complex.

	Trial #1 ($M^{-1}s^{-1}$)		Trial #2 ($M^{-1}s^{-1}$)		Trial #3 ($M^{-1}s^{-1}$)		Average ($M^{-1}s^{-1}$)		
Complex	Rate Constant	St.Err.	Rate Constant	St.Err.	Rate Constant	St.Err.	Rate Constant	St.Err.	St.Dev.
ET0	7023	13	7308	13	7200	13	7177	13	144
ET1	4708	10	4189	10	4788	10	4562	10	325
ET2	3032	9	3088	9	3124	9	3081	9	47
ET3	1260	9	1296	9	1282	9	1279	9	18
ET4	451	10	445	10	450	9	449	10	4
ET5	366	8	373	8	374	8	371	8	4
ET6	403	7	359	7	412	7	391	7	29
ET7	472	7	517	8	516	7	502	7	26
ET8	3710	12	3738	12	3870	12	3773	12	86
ET9	4323	15	4361	15	4166	15	4284	15	104
ET10	3128	12	3198	12	3181	13	3169	12	37
ET11	3827	15	3750	15	3844	15	3807	15	50

Table S14 Rate constant and standard error data copied from Origin Lab fitting of kinetics traces shown in **Figure S17** of internal toehold complexes in low (1.25 mM) $MgCl_2$ concentrations. Standard deviations were calculated via excel after copying and pasting data from Origin. Internal toehold complexes are represented by codes of the form ITx, where x is the number of auxiliary arms of the complex.

	Trial #1 ($M^{-1}s^{-1}$)		Trial #2 ($M^{-1}s^{-1}$)		Trial #3 ($M^{-1}s^{-1}$)		Average ($M^{-1}s^{-1}$)		
Complex	Rate Constant	St.Err.	Rate Constant	St.Err.	Rate Constant	St.Err.	Rate Constant	St.Err.	St.Dev.
IT0	5689	12	5649	12	5690	11	5676	12	23
IT1	3150	11	3200	11	3118	11	3156	11	41
IT2	1853	8	1802	8	1810	8	1822	8	27
IT3	1696	9	1658	9	1663	10	1672	9	21
IT4	1280	8	1237	8	1245	8	1254	8	23
IT5	958	8	954	9	977	9	963	9	12
IT6	24038	160	24870	154	24295	159	24401	158	426
IT7	17822	196	17679	198	17874	201	17792	198	101
IT8	20586	180	20120	172	21365	193	20690	182	629
IT9	19619	204	19339	192	19111	211	19356	202	255
IT10	17971	37	18272	38	17615	37	17953	37	329

Table S15 Rate constant and standard error data copied from Origin Lab fitting of kinetics traces shown in **Figure S18** of external toehold complexes in high (125 mM) $MgCl_2$ concentrations. Standard deviations were calculated via excel after copying and pasting data from Origin. External toehold complexes are represented by codes of the form ETx, where x is the number of auxiliary arms of the complex.

	Trial #1 ($M^{-1}s^{-1}$)		Trial #2 ($M^{-1}s^{-1}$)		Trial #3 ($M^{-1}s^{-1}$)		Average ($M^{-1}s^{-1}$)		
Complex	Rate Constant	St.Err.	Rate Constant	St.Err.	Rate Constant	St.Err.	Rate Constant	St.Err.	St.Dev.
ET0	7.63E+06	80256	8.58E+06	83087	7.88E+06	70650	8.03E+06	77998	493701
ET1	3.69E+06	27950	4.10E+06	29829	4.03E+06	29284	3.94E+06	29021	218633
ET2	3.78E+06	28076	3.83E+06	27446	3.87E+06	29170	3.83E+06	28231	45331
ET3	2.29E+06	17457	2.44E+06	18893	2.44E+06	18728	2.39E+06	18359	83970
ET4	2.44E+06	22173	2.37E+06	19957	2.48E+06	21818	2.43E+06	21316	53667
ET5	1.73E+06	12121	1.80E+06	13147	1.78E+06	12824	1.77E+06	12698	35858
ET6	2.33E+06	28576	2.33E+06	29605	2.38E+06	30097	2.35E+06	29426	27291
ET7	1.12E+06	6103	1.01E+06	5108	1.28E+06	10295	1.14E+06	7169	136560
ET8	7.90E+05	4726	7.79E+05	4634	8.10E+05	4928	7.93E+05	4762	15748
ET9	6.10E+05	3088	4.81E+05	2100	5.93E+05	2972	5.61E+05	2720	70110
ET10	6.29E+05	3413	7.09E+05	4252	7.35E+05	4345	6.91E+05	4003	55568
ET11	4.40E+05	2187	4.27E+05	2280	4.29E+05	2188	4.32E+05	2218	6987

Table S16 Rate constant and standard error data copied from Origin Lab fitting of kinetics traces shown in **Figure S19** of internal toehold complexes in high (125 mM) $MgCl_2$ concentrations. Standard deviations were calculated via excel after copying and pasting data from Origin. External toehold complexes are represented by codes of the form ITx, where x is the number of auxiliary arms of the complex.

	Trial #1 ($M^{-1}s^{-1}$)		Trial #2 ($M^{-1}s^{-1}$)		Trial #3 ($M^{-1}s^{-1}$)		Average ($M^{-1}s^{-1}$)		
Complex	Rate Constant	St.Err.	Rate Constant	St.Err.	Rate Constant	St.Err.	Rate Constant	St.Err.	St.Dev.
IT0	1.02E+07	2E+5	1.01E+07	2E+5	1.09E+07	2E+5	1.04E+07	2E+5	446340
IT1	6.60E+06	70867	6.45E+06	63018	7.05E+06	78885	6.70E+06	70923	309721
IT2	5.76E+06	75063	5.26E+06	67149	6.11E+06	83443	5.71E+06	75218	423454
IT3	3.47E+06	30056	3.56E+06	32703	3.54E+06	32273	3.52E+06	31677	50474
IT4	3.71E+06	36701	4.83E+06	54823	4.17E+06	43260	4.24E+06	44928	564828
IT5	2.88E+06	22023	2.82E+06	21229	2.81E+06	20340	2.84E+06	21197	35218
IT6	2.30E+06	19080	2174410	18106	2237120	19237	2.24E+06	18808	62246
IT7	1.67E+06	12065	1636370	12319	1720290	12660	1.68E+06	12348	42061
IT8	1.72E+06	15434	2.06E+06	20530	1.72E+06	15661	1.84E+06	17209	192353
IT9	1.17E+06	8671	1.11E+06	8591	1.17E+06	9032	1.15E+06	8764	37367

Kinetic Curve Fitting Equation

All kinetics data were fit using this equation assuming bimolecular reaction kinetics.

$$f = F_{Max} - \frac{(F_{Max} - F_{Baseline})}{(1 + 60 \times k \times C \times (t - t_0))} \quad \textbf{(1)}$$

Where F_{Max} is the maximum fluorescence, $F_{Baseline}$ is the baseline fluorescence, k is the rate constant, C is the concentration of both species at the beginning of the reaction, t_0 is the start time and t is the reaction time.

Alternative Plots

Figure 4 of the manuscript contains data points that are difficult to distinguish due to the linear scale. While the linear scale is helpful for seeing the small changes in data that are important for discussing, this log plot in **Figure S20** helps show the continuing drop of reaction rate constant at higher auxiliary arm counts. It also more clearly depicts the three-order magnitude difference between the external toehold reporter complex control with zero auxiliary arms and the constrained complex with five auxiliary arms.

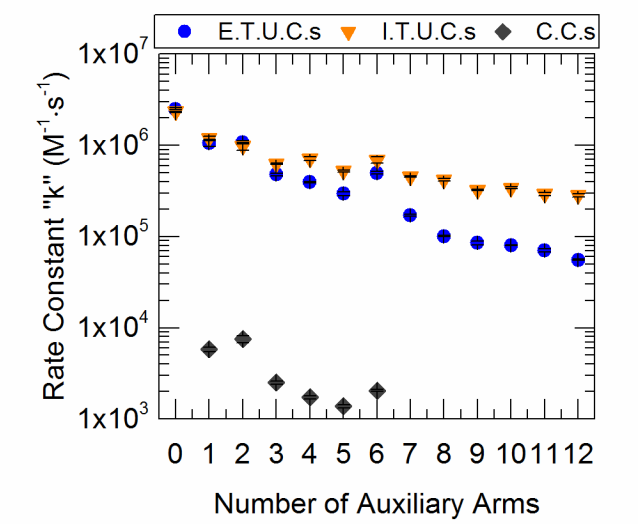

Figure S20 A semi-log plot of auxiliary arms versus rate constant. External toehold Unconstrained complexes (E.T.U.C.s) are shown as blue circles, internal toehold unconstrained complexes (I.T.U.C.s) are shown as orange triangles, and constrained complexes (C.C.s) are shown as dark gray diamonds.

Figure 5 of the manuscript shows the differences in rate constants with the incremental addition of each arm in order to show a pattern in the data. **Figure S21** shows that same pattern but in the form of a ratio. The ratio is the change of rate constant divided by the rate constant of the control complex.

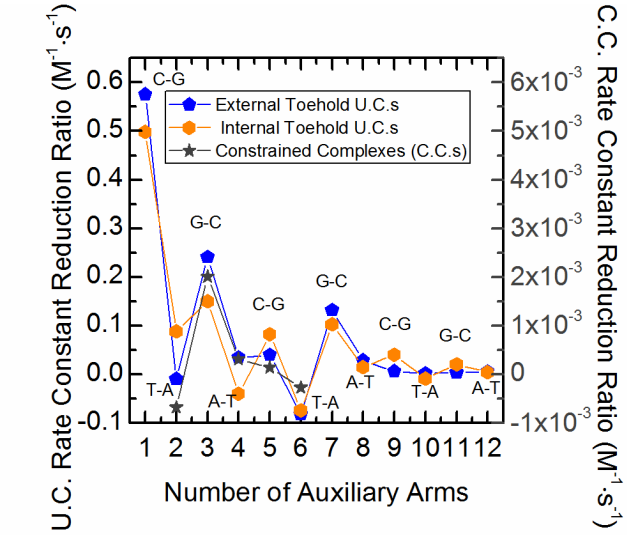

Figure S21 A plot of the rate constant reduction by ratio is provided in addition to the rate constant change plot which is found in the manuscript as **Figure 5**.

NUPACK Structures

Unconstrained External Toehold Complexes

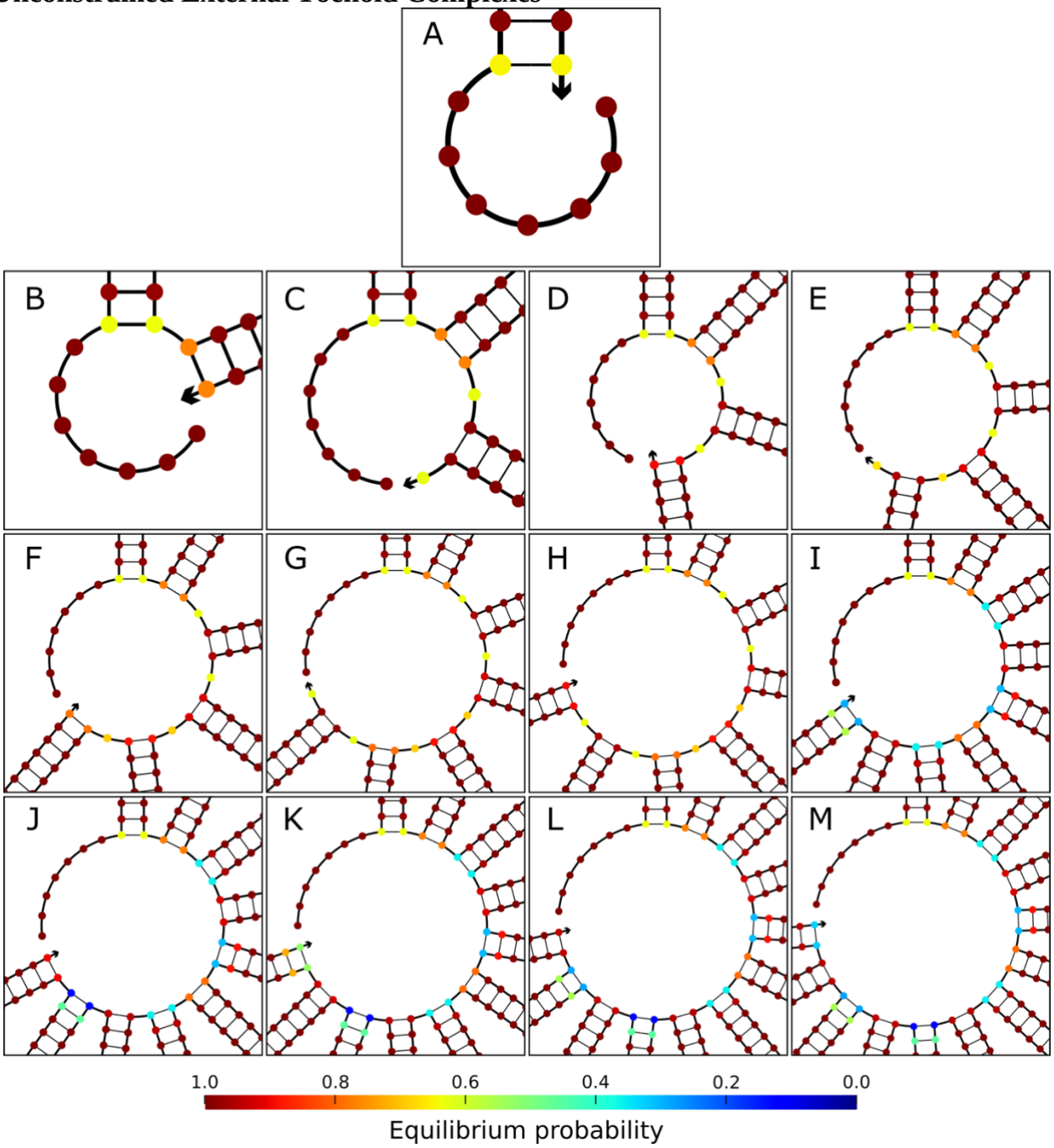

Figure S22 Minimum Free Energy (MFE) diagrams of unconstrained external toehold complex junctions from NUPACK[10-14]. **Figures S22A-M** illustrate external toehold complexes of 0-12 auxiliary arms respectively. Diagrams were all calculated using NUPACK's online utilities MFE tool. NUPACK settings included DNA as the as the nucleic acid material, 25C as the temperature, 0.05M Na and 0.0125 Mg salt concentrations, with dangle treatment set to "some". Diagrams do not detail any substantial differences in toehold nucleotide availability. Due to the importance of the junction and negligible changes of the auxiliary arms, the junctions are magnified, omitting full structures, creating better visuals for a conducive comparison of different structures.

Unconstrained Internal Toehold Complexes

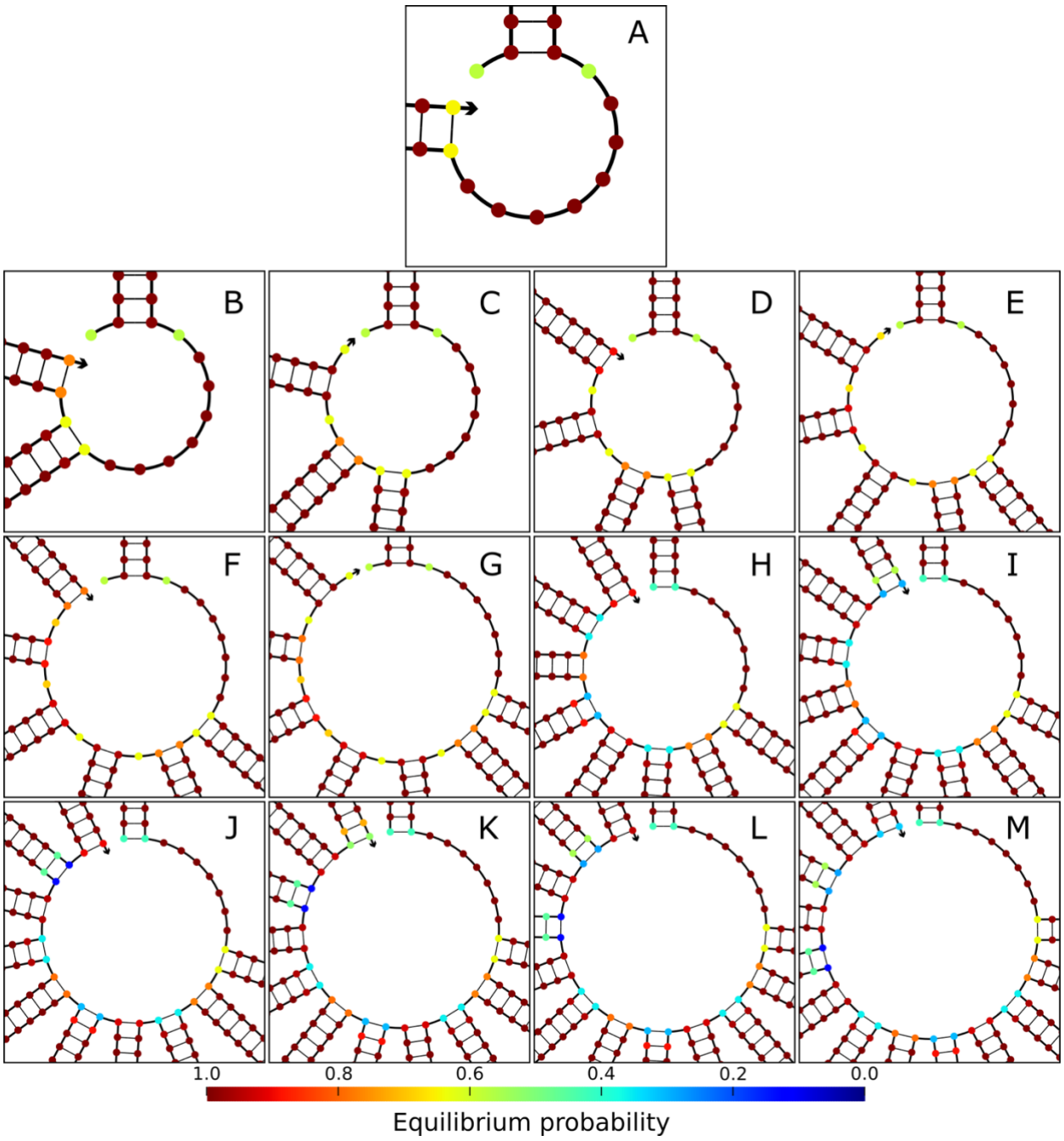

Figure S23 Minimum Free Energy (MFE) diagrams of unconstrained internal toehold complex junctions from NUPACK. **Figures S23A-M** illustrate internal toehold complexes of 0-12 auxiliary arms respectively. Diagrams were all calculated using NUPACK's online utilities MFE tool. NUPACK settings included DNA as the nucleic acid material, 25C as the temperature, 0.05M Na and 0.0125 Mg salt concentrations, with dangle treatment set to "some". Diagrams do not detail any substantial differences in toehold nucleotide availability. Due to the importance of the junction and negligible changes of the auxiliary arms, the junctions are magnified, omitting full structures, creating more conducive visuals for comparison of different structures.

Constrained Toehold Complexes

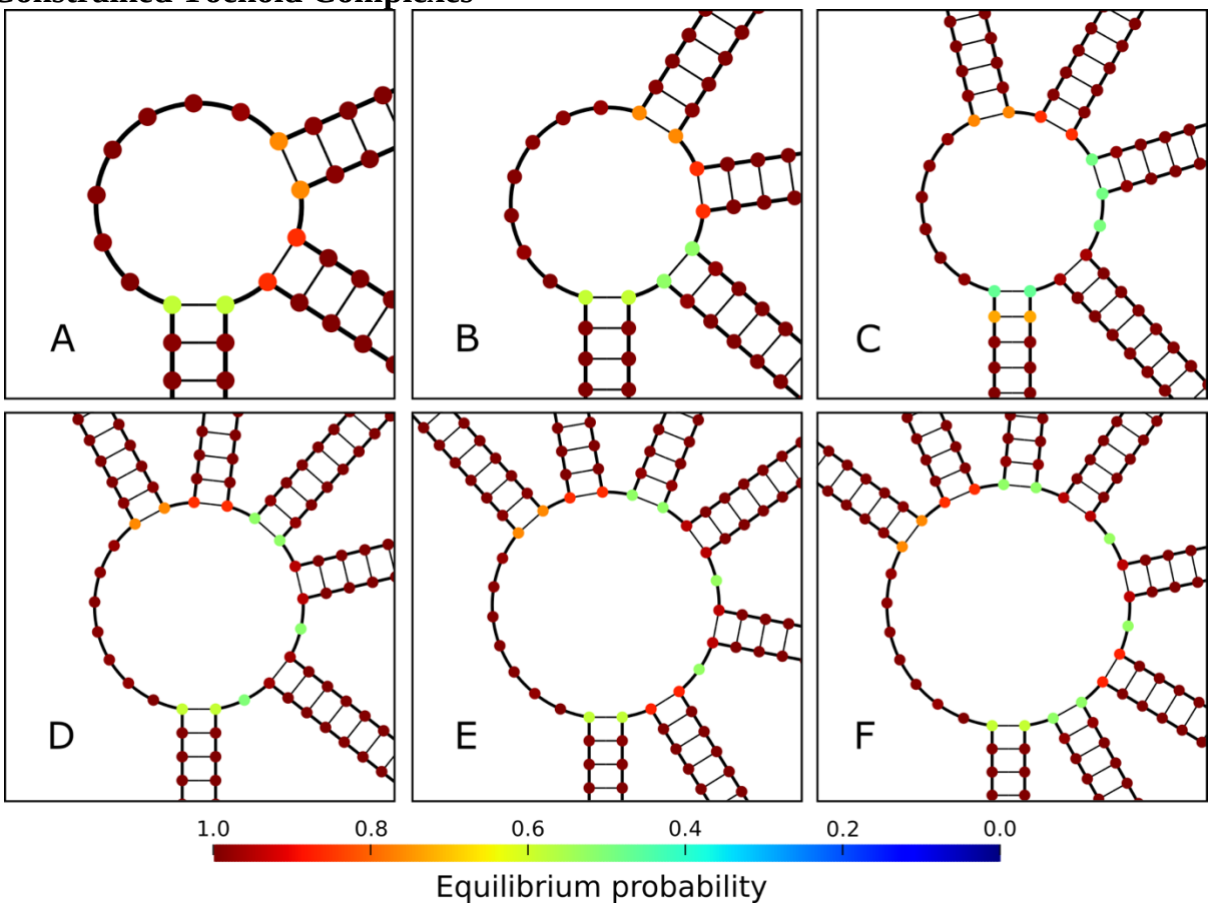

Figure S24 Minimum Free Energy (MFE) diagrams of constrained complex junctions from NUPACK. **Figures S24A-F** illustrate internal toehold complexes of 1-6 auxiliary arms respectively. Diagrams were all calculated using NUPACK's online utilities MFE tool. NUPACK settings included DNA as the nucleic acid material, 25C as the temperature, 0.05M Na and 0.0125 Mg salt concentrations, with dangle treatment set to "some". Diagrams do not detail any substantial differences in toehold nucleotide availability. Due to the importance of the junction and negligible changes of the auxiliary arms, the junctions are magnified, omitting full structures, creating more conducive visuals for comparison of different structures.

Programmable Sterics

Gel Analysis

In **Figures 10** and **11** of the manuscript, steric moieties are demonstrated to be programmable by adding and subtracting steric moieties using strand displacement reactions. The reactions in step one of these figures are shown again here in **Figure S25A** and illustrate the steric transformations before the invasion reactions occur in step two. To ensure that intermediate structures are formed as presumed during step one, **Figure S25B** shows a polyacrylamide gel with the relevant species. Lanes one and ten of the gel are empty. Lane two shows the purified products of the P5 reaction 24 hours after the reactants were introduced. Separately purified ET1 and steric moiety (with 20 bp arms) complexes were run in lanes three and five respectively. These bands match the bands in lane two as expected. Lane four shows a band with the P5 complex, which is not seen in lane two, suggesting a full reaction occurred. Lane seven shows the purified products of the P1 reaction 24 hours after mixing a 1:1.3 ratio of P1 to steric moiety. The left most band matches with the separately purified ET5 complex band run in lane six and the small right band confirms an excess of steric moiety that was also separately purified and run in lane eight. A separately purified P1 complex was run in lane nine and no evidence of residual P1 reactant is evident in the lane seven.

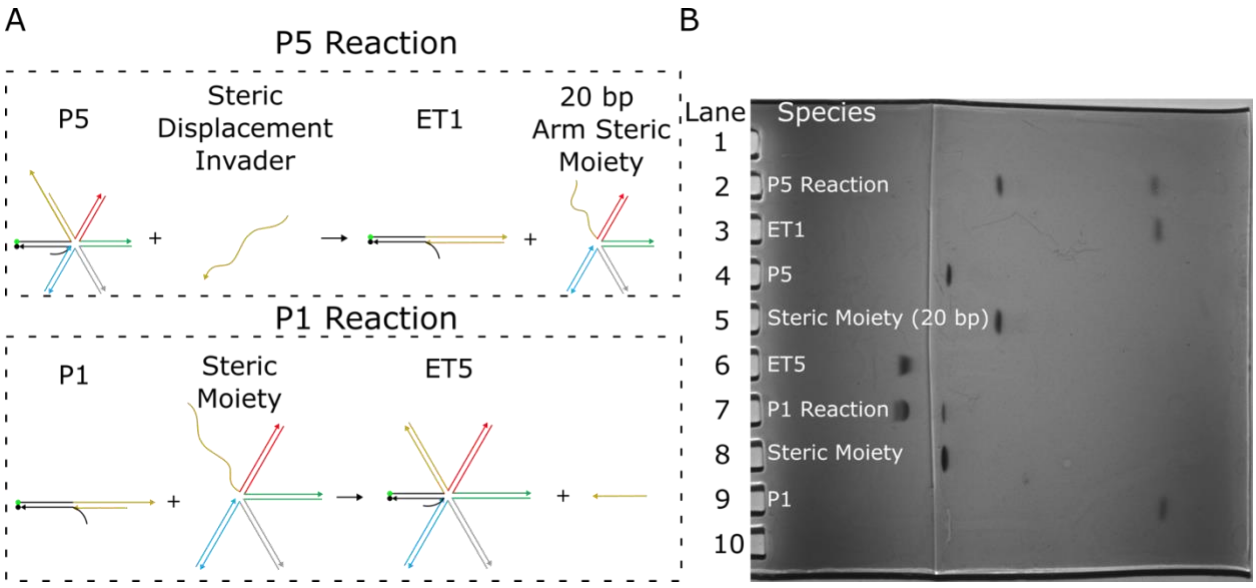

Figure S25 Schematics and polyacrylamide gel verification of programmable steric complex reactions. **(A)** The transformation of a P5 to an ET1 complex is shown in the upper dashed box. The transformation of a P1 to an ET5 complex is shown in the lower dashed box. **(B)** A stacked 8%-12% polyacrylamide gel shows reactions depicted in **A** within lanes two and seven and separately purified components of these reactions in the other occupied lanes.

Steric Moiety Invasion Interference

In **Figure 11** of the manuscript an experiment is presented to demonstrate that a five auxiliary arm complex can be converted into a one arm complex, to increase the overall reaction kinetics. The gel analysis in **Figure S25** shows that there was full conversion of the five-arm complex to the one-arm complex, yet the rate constant did not resemble the faster kinetics of a one-arm complex. After investigating, the steric moiety stripped in step one of the reaction, depicted in part **A** of **Figure 11** or more conveniently in part **A** of **Figure S26,** was found to be interacting with the invader strand added in step two of the reaction. A NUPACK minimum free energy structure of the invader and steric moiety interaction is shown in **Figure 11B**. This interaction helps to decrease the overall reaction rate constant so that the full reaction rate constant of the ET1 complex cannot be recouped.

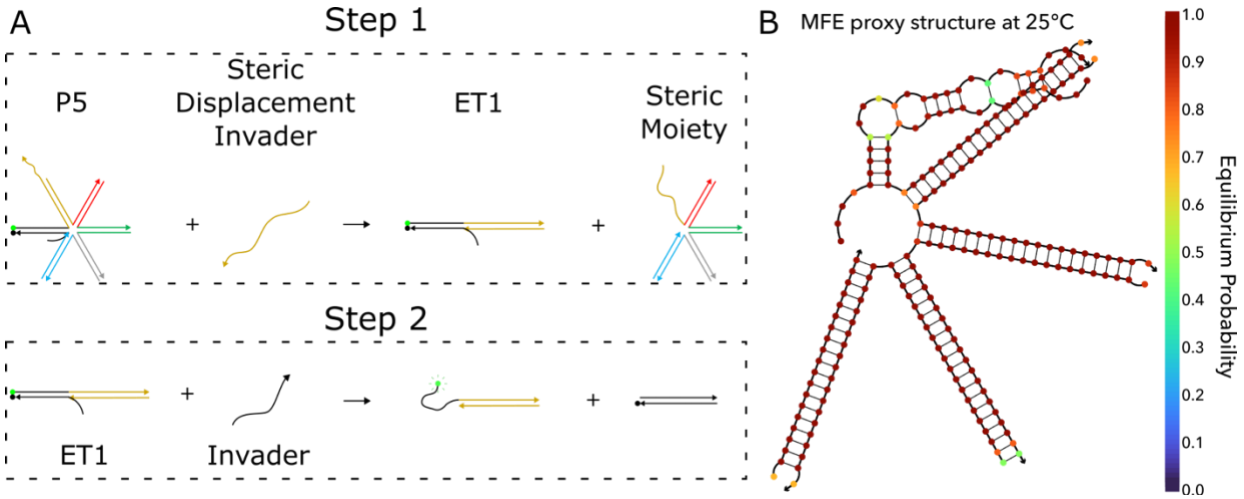

Figure S26 Reaction schematics of sterically programmed P5 complex and minimum free energy structure of the steric moiety and invader strand. **(A)** Schematics of reaction components are re-featured from **Figure 11** of the manuscript. **(B)** A minimum free energy (MFE) structure of the steric moiety complex shown on the right of step one in **A** and the invader of complex ET1 shown on the left in **A**.

References:

(1) Wang, X.; Seeman, N. C. Assembly and Characterization of 8-Arm and 12-Arm DNA Branched Junctions. *Journal of the American Chemical Society* **2007**, *129* (26), 8169-8176. DOI: 10.1021/ja0693441.
(2) Zhang, D. Y.; Turberfield, A. J.; Yurke, B.; Winfree, E. Engineering entropy-driven reactions and networks catalyzed by DNA. *Science* **2007**, *318* (5853), 1121-1125.
(3) Snodin, B. E. K.; Randisi, F.; Mosayebi, M.; Šulc, P.; Schreck, J. S.; Romano, F.; Ouldridge, T. E.; Tsukanov, R.; Nir, E.; Louis, A. A.; et al. Introducing improved structural properties and salt dependence into a coarse-grained model of DNA. *The Journal of Chemical Physics* **2015**, *142* (23), 234901. DOI: 10.1063/1.4921957.
(4) Šulc, P.; Romano, F.; Ouldridge, T. E.; Rovigatti, L.; Doye, J. P. K.; Louis, A. A. Sequence-dependent thermodynamics of a coarse-grained DNA model. *The Journal of Chemical Physics* **2012**, *137* (13), 135101-135101. DOI: 10.1063/1.4754132.
(5) Ouldridge, T. E.; Šulc, P.; Romano, F.; Doye, J. P. K.; Louis, A. A. DNA hybridization kinetics: zippering, internal displacement and sequence dependence. *Nucleic Acids Research* **2013**, *41* (19), 8886-8895. DOI: 10.1093/nar/gkt687.
(6) Rovigatti, L.; Šulc, P.; Reguly, I. Z.; Romano, F. A comparison between parallelization approaches in molecular dynamics simulations on GPUs. *Journal of Computational Chemistry* **2015**, *36* (1), 1-8. DOI: https://doi.org/10.1002/jcc.23763.
(7) Ouldridge, T. E.; Louis, A. A.; Doye, J. P. K. Structural, mechanical, and thermodynamic properties of a coarse-grained DNA model. *The Journal of Chemical Physics* **2011**, *134* (8), 085101. DOI: 10.1063/1.3552946.
(8) Poppleton, E.; Romero, R.; Mallya, A.; Rovigatti, L.; Šulc, P. OxDNA.org: a public webserver for coarse-grained simulations of DNA and RNA nanostructures. *Nucleic Acids Research* **2021**, *49* (W1), W491-W498. DOI: 10.1093/nar/gkab324 (acccessed 8/13/2022).
(9) Suma, A.; Poppleton, E.; Matthies, M.; Šulc, P.; Romano, F.; Louis, A. A.; Doye, J. P. K.; Micheletti, C.; Rovigatti, L. TacoxDNA: A user-friendly web server for simulations of complex DNA structures, from single strands to origami. *Journal of Computational Chemistry* **2019**, *40* (29), 2586-2595. DOI: https://doi.org/10.1002/jcc.26029.
(10) Zadeh, J. N.; Steenberg, C. D.; Bois, J. S.; Wolfe, B. R.; Pierce, M. B.; Khan, A. R.; Dirks, R. M.; Pierce, N. A. NUPACK: Analysis and design of nucleic acid systems. *Journal of computational chemistry* **2011**, *32* (1), 170-173.
(11) Dirks, R. M.; Pierce, N. A. A partition function algorithm for nucleic acid secondary structure including pseudoknots. *Journal of computational chemistry* **2003**, *24* (13), 1664-1677.
(12) Dirks, R. M.; Pierce, N. A. An algorithm for computing nucleic acid base-pairing probabilities including pseudoknots. *Journal of computational chemistry* **2004**, *25* (10), 1295-1304.
(13) Dirks, R.; Bois, J.; Schaeffer, J.; Winfree, E.; Pierce, N. Thermodynamic Analysis of Interacting Nucleic Acid Strands. *SIAM Review* **2007**, *49* (1), 65-88. DOI: 10.1137/060651100.
(14) Fornace, M. E.; Porubsky, N. J.; Pierce, N. A. A unified dynamic programming framework for the analysis of interacting nucleic acid strands: Enhanced models, scalability, and speed. *ACS Synthetic Biology* **2020**, *9* (10), 2665-2678.